

STIS Cycle 9 Calibration Close-out Report

Charles R. Proffitt and James Davies on behalf of the

Spectrographs Group: Thomas M. Brown, Ivo Busko (Software Science Group), Rosa Diaz-Miller, Ron Downes, Linda Dressel, Paul Goudfrooij, Phil Hodge (Software Science Group), Jessica Kim Quijano, Howard Lanning (former group member), Claus Leitherer (former group member), Chris Long (Engineering Team), Jesús Maíz-Apellániz, Grace Mitchell (former group member), Bahram Mobasher, Mike Potter, Kailash Sahu, David Stys, Jeff Valenti, Nolan Walborn (former group member).

February 28, 2003

ABSTRACT

We summarize the status of the Cycle 9 calibration program for the Space Telescope Imaging Spectrograph (STIS) based on three years of on-orbit calibration observations.

1. Introduction

Cycle 9 was the third HST Cycle for which STIS is available, and as our understanding of the instrument has matured, the primary emphasis of the calibration program has shifted from programs that define the basic operation and fundamental calibration of the instrument, to programs that monitor instrument health and stability. However, there were still a number of special calibration programs that were implemented to expand our understanding of the basic calibration and to test new ways of using STIS.

In Cycle 9, a total of 30 calibration proposals executed over the period between June 2000 and September 2001 to monitor the spectrograph's performance and improve its

characterization. The definition and oversight of this program was initially led by Paul Goudfrooij, assisted by Rosa Diaz-Miller. In October of 2001, Charles Proffitt took over as the lead for STIS calibration efforts, assisted at first by Rosa Diaz-Miller, and later by James Davies.

The initially approved Cycle 9 calibration plan included 84 prime external and 1917 internal orbits. Most of these internal orbits are true internal visits that can be executed during occultations of HST's primary target. However, the 232 internal orbits allocated to programs 8841 and 8851 are individually too large to fit into occultations, and these have to be executed as pure parallel observations. A new 3 orbit program was added to the Cycle 9 plan later in the cycle, after approval by the director's office. This was 8891, "Test of STIS End of Slit Pseudo-Aperture Locations," that performed an end-to-end systems test of the use of the new pseudo-aperture positions which were implemented to mitigate CTE losses. This program also verified the exact aperture positions that had been measured in the Cycle 8 program 8799.

While Cycle 9 nominally ran from July 2000 through June 2001, many Cycle 9 calibration monitoring programs were planned to cover the period from July 1, 2000 through August 31, 2001. This extended period of coverage for some Cycle 9 programs allowed Cycle 10 calibration monitoring programs to be submitted and implemented well after the submission deadline for Cycle 10 GO programs. This reduced the peak workload for planning and scheduling activities, and also allows each cycle's calibration program to be better tailored to the actual needs of the submitted GO programs.

Cycle 9 also saw the failure of the STIS side-1 electronics on 16 May 2001. STIS was brought back up using the redundant side-2 electronics in early July 2001, and several special calibration proposals were implemented to support the recommissioning of the instrument. While these special calibration proposals are, for some purposes, considered part of Cycle 9 calibration, they will not be discussed here.

The majority of calibration programs in this cycle are routine programs that have been established to monitor the stability of STIS and proactively search for problems that could impact the quality of the data obtained. Most of them continue monitoring started in Cycles 7 and 8. These include monitors of aperture, focus and MSM stability, as well as monitors of sensitivity, acquisition accuracy, and lamp flux degradation. Also included are checks of basic detector performance and flat-fields. Extensive internal exposures of CCD dark and bias frames are included to allow production of needed reference files.

Two new monitoring programs were added this cycle and will be continued in subsequent cycles. These are 8851 and 8854, which measure the degradation of charge transfer efficiency for point sources.

Special, one-time calibrations in the initial plan included six purely CCD programs and one that used both the CCD and the MAMA detectors. The special CCD programs include 8842 (with observations of imaging flux and PSF standards), 8839 (which explored CTE effects for observations of extended targets), 8844 (which obtained very

deep spectroscopic PSFs for specialized applications), 8850 (which obtained deep wave-cal exposures for select modes), 8852 (a measurement of CCD window ghosts), and 8853 (which checked for residual effects after severe over illumination of the CCD). Program 8849, “Faint Standards Extension,” is designed to improve the spectroscopic flux calibration of faint standard stars, needed for MAMA imaging and COS calibration work.

Table 1. Summary of orbit allocation and use during the Cycle 9 calibration of STIS. This table does not include the programs associated with the side-2 recovery of STIS.

Cycle 9 Orbits	External Orbits	Internal Orbits
Allocated	77	1917
Executed	82	1506
Withdrawn	3	360
Failed	0	24
Repeated	0	11
Active	0	0

The results of Cycle 9 calibration proposals are summarized in Table 2. Details for each proposal are given in the page number listed in the last column. For ease of management of the calibration program, the proposals were divided into logical groups, such as CCD Monitoring or MAMA Monitoring. For the Time Used (columns 3 and 4), we have listed both the executed orbits, and in square brackets [] the allocated orbits, on a proposal by proposal basis. To keep the size of the Phase 2 proposals manageable for implementation purposes, particularly for the routine monitoring proposals (e.g., the CCD Dark Monitor), it was sometimes necessary to split one particular aspect of the calibration into several separate Phase 2 proposals. While these were tracked separately, and are presented as separate proposals in the table, they are in fact parts of the same calibration and are not treated as separate entities in the detailed forms following the table. The forms summarize the following five items:

1. Execution: Success and frequency of proposal observations.
2. Summary of Goals: Purpose of calibration
3. Summary of Analysis: Highlights of the results and products, including references for detailed analysis, procedures and/or requirements.
4. Accuracy Achieved: Accuracy of the result or data processed using the calibration product.
5. Continuation Plans: Follow-up calibration proposals or analysis.

The primary products of the Cycle 9 calibration program were calibration reference files delivered to the OPUS Pipeline, STIS Instrument Science Reports (ISRs), STIS Technical Instrument Reports (TIRs), and updates to the STIS Instrument Handbook (IHB). The reference file products for individual proposals are identified by their suffix, listed in the Reference File History site (http://www.stsci.edu/instruments/stis/calibration/reference_files/oref.html). The STIS ISRs, TIRs, and IDT analysis reports are referenced by number (e.g., ISR 90-28). The author and date may be found in Appendix A. TIRs are only available from the STIS internal web site, which has restricted access.

The calibration programs described here also contributed to a number of papers at the *2002 HST Calibration Workshop* (Arribas, Koekemoer, & Whitmore 2002). These papers are also listed in Appendix A.

Analysis of STIS calibration data now tends to span multiple cycles, and the resulting calibration products depend on data from a number of programs. Important recent improvements in STIS calibration that were significantly enabled by Cycle 9 calibration data include:

1. Implementation of the E1 aperture positions for the reduction of CTE effects.
2. Installation in the STIS calibration pipeline of time-dependent sensitivity corrections for 1st order MAMA modes.
3. Revision of CCD imaging throughputs to allow accurate zero points to be determined for 50CCD and F28X50LP imaging.
4. Significantly improved characterization of the time dependant degradation in charge transfer efficiency (CTE).

2. CCD Monitoring and Detector Calibration

Table 2. STIS Cycle 9 Calibration Closure Summary

ID	Proposal Title	Time Used (orbits)		Products	Accuracy Achieved	Page
		executed	[allocated]			
		“External”	“Internal”			
CCD Monitoring and Detector Calibration						
8836	CCD Performance Monitor		42 [42]	BIA and DRK <i>reference files</i>	gain measured to 1% (unbinned), 1%-3% (binned); read noise measured to 1%-3% (unbinned), 2%-4% (binned)	page 8
8837 8864	CCD Dark Monitor		365 [420] 256 [420]	DRK <i>reference files</i> ; Cal. workshop paper (Brown).	S/N ~7 (side-1), 6 (side-2) dark current ~0.0041 electrons/s/pixel	page 9
8838 8865	CCD Bias Monitor		183 [213] 128 [213]	BIA <i>reference files</i>	S/N > 1.0 per pixel	page 10
8840	CCD Read Noise Monitor		24 [28]	<i>IHB</i> and web page updates	+/-0.05 DN	page 12
8841	CCD Hot Pixel Annealing		156 [168]	<i>monthly reports</i> ; <i>web</i> ; <i>IHB updates</i> ; ISR 2001-003 (Brown); <i>Cal. Workshop paper</i> (Brown).		page 13
8845	CCD Spectroscopic Flats		53 [79]	PFL <i>reference files</i> .	RMS residuals at least as small as 0.3% can be obtained.	page 15
8846	CCD Imaging Flats		17 [18]		RMS differences from previous pflat are about 0.35%.	page 16
8847	CCD Full-Field Sensitivity	2 [3]		<i>ISR</i> in preparation (Mobasher & Davies.	< 1% for stars $m > 20$ over the full field.	page 17
8848	CCD Dispersion Solutions		4 [4]			page 19
8851	CCD Sparse-Field CTE Internal		64 [64]	<i>ISR</i> in preparation (Bohlin & Goudfrooij); <i>Cal. Workshop paper</i> (Goudfrooij)	1% for signal levels > 200 electrons at center of detector	page 20
8854	CCD Sparse-Field CTE External	8 [6]		<i>ISR</i> in preparation (Goudfrooij & Potter); <i>Cal. Workshop paper</i> (Goudfrooij)	1% for signal levels > 200 electrons at center of detector	page 22
8855	Slit Wheel Repeatability		1 [1]			page 24
8856	CCD Sensitivity Monitor	6 [6]		<i>ISR</i> in preparation (Walborn & Stys) <i>Cal. Workshop paper</i> (Bohlin).	rms scatter is consistent with previous cycles	page 27

Table 2. STIS Cycle 9 Calibration Closure Summary

ID	Proposal Title	Time Used (orbits)		Products	Accuracy Achieved	Page
		executed	[allocated]			
		“External”	“Internal”			
CCD Special Calibration Programs						
8842	CCD PSF Library	3 [3]		<i>IHB</i> ; web interface to library <i>Cal. Workshop paper</i> (Proffitt).	revised CCD flux calibration ~3%	page 28
8844	Deep Spatial/Spectral PSF Calibration	11 [7]		Cal. Workshop papers (Gull; Grady).	Still under evaluation.	page 29
8850	Deep CCD/G750M Wavecals		3 [2]		N/A	page 30
8852	Measurement of CCD Window Ghost in Spectrographic Mode	2 [2]	3 [0]	<i>Quicklook Reports 63 & 65</i> ;	ghosts modelled and subtracted with < 10% error	page 31
8839	CTE for Extended Targets	4 [4]		CTI measurements for <i>ISR</i> .	see plots	page 32
8853	CCD Residual Images after Overillumination	2 [2]	3 [3]			page 35
8891	Test of STIS End of Slit Pseudo-Aperture Locations	3 [3]		Revised reference files.		page 37
MAMA Monitoring and Detector Calibration						
8843	MAMA Dark Monitor		170 [208]	<i>DRK reference files</i> ; <i>Web</i> and <i>IHB</i> updates <i>Cal Workshop paper</i> (Proffitt).	mean NUV dark rate between 1100 and 1800 cnts/s	page 39
8857	MAMA Sensitivity and Focus Monitor	19 [22]		Cal. Workshop papers (Bohlin; Stys).		page 41
8858	MAMA Full-Field Sensitivity	6 [6]		<i>ISR</i> in preparation (Davies & Mobasher); <i>Cal. Workshop paper</i> (Proffitt).	RMS scatter, bright stars: NUV-SRF2 1%; FUV-25MAMA 3%.	page 43
8859	MAMA Dispersion Solutions		10 [10]			page 46
8860	MAMA Fold Distribution		4 [4]	<i>Engineering White Paper</i> 02-030.	No degradation: measurements within 20% of past results.	page 47
8862	MAMA FUV flats		10 [10]	<i>PFL reference file</i> ; TIR 2002-03 (Brown & Davies)..	expected 1% per low resolution element	page 49
8863	MAMA NUV flats		10 [10]	<i>PFL reference file</i> ; TIR 2002-03 (Brown & Davies).	expected 1% per low resolution element	page 50

Table 2. STIS Cycle 9 Calibration Closure Summary

ID	Proposal Title	Time Used (orbits)		Products	Accuracy Achieved	Page
		executed	[allocated]			
		“External”	“Internal”			
MAMA Special Calibration Programs						
8849	Faint Standards Extension (FASTEX)	16	[16]	<i>Cal. Workshop paper</i> (Bohlin).		page 51
Totals						
TOTAL ORBITS EXECUTED		82	1506			
Number of Allocated Orbits		[80]	[1917]			

Proposal ID 8836: CCD Performance Monitor

Execution	Dark frames in 2x2 binning mode were taken once in Sep 2000. All other observations were made twice during the cycle, in Dec 2000 and May 2001. The last measurements were made shortly before the loss of the side-1 electronics.
Summary of Goals	Measure bias level, read noise, and gain at many combinations of gain and binning to update the CCD reference files as needed. Make bias and dark reference files at the lesser used combinations of gain and binning not covered by the daily dark and bias programs. Measure CTE using the EPER method.
Summary of Analysis	The analysis is the same as for previous cycles, described in ISR 98-31 and Kimble et al 2000. The products include ccd, bia, and drk reference files. The measurements for the CCD reference files are given in Table 3.
Accuracy Archived	Gain was measured to 1% for the unbinned pixel format, and from 1% to 3% for the binned pixel formats. Read noise was measured to 1% to 3% for the unbinned pixel format, and from 2% to 4% for the binned pixel formats. Bias level was measured to 1 ADU.
Continuation Plans	Continued without change in Cycle 10 program 8900.

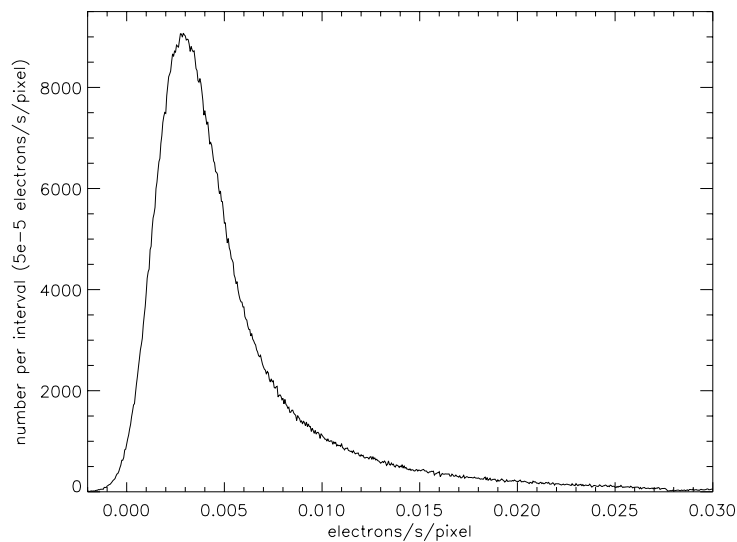
Table 3. CCD bias level, gain, and readnoise in Dec 2000 & May 2001

Month	Gain	Binning	Bias Level (ADU)	Gain (electrons/ADU)	Read Noise (electrons)
Dec	1	1x1	1345	1.006+-0.007	4.46+-0.09
May	1	1x1	1355	1.002+-0.010	4.57+-0.07
Dec	1	1x2	1349	0.975+-0.007	4.29+-0.07
May	1	1x2	1351	0.989+-0.011	4.05+-0.09
Dec	1	2x1	1135	0.999+-0.009	3.81+-0.06
May	1	2x1	1146	1.014+-0.017	3.84+-0.07
Dec	1	2x2	1134	0.991+-0.023	3.79+-0.13
May	1	2x2	1144	1.010+-0.017	3.82+-0.12
Dec	1	4x1	1029	0.997+-0.022	3.86+-0.13
May	1	4x1	1038	1.019+-0.027	3.89+-0.20
Dec	1	4x2	1030	1.036+-0.030	4.13+-0.16
May	1	4x2	1040	0.967+-0.023	3.81+-0.13
Dec	2	1x1	1565	1.992+-0.009	5.67+-0.13
May	2	1x1	1568	1.999+-0.015	5.78+-0.14
Dec	4	1x1	1513	4.107+-0.059	7.75+-0.21
May	4	1x1	1514	4.008+-0.027	7.61+-0.14
Dec	8	1x1	1554	8.117+-0.087	11.31+-0.17
May	8	1x1	1554	8.119+-0.071	12.46+-0.18

Proposal ID 8837 & 8864: CCD Dark Monitor

Execution	Executed twice per day (8837 in the first half of the cycle, 8864 in the second half) except during the period when STIS was safed (May 17 to July 11, 2001).
Summary of Goals	Produce weekly dark reference files from a series of long dark exposure (1100 s). Take several short dark exposures daily, which observers can use to update the hot pixel intensities in the weekly dark reference files using the stsdas script daydark.
Summary of Analysis	Data taken between monthly anneals is combined to produce a baseline dark image. Weekly reference dark files are made by using weekly data to update the hot pixels in the baseline dark image. The bias reference image for the corresponding time range is used to remove the bias from the dark reference frame. When STIS was recovered in July 2001 using side-2 electronics, it became necessary to scale the dark exposures to compensate for the varying temperature of the CCD detector. Scaling factors typically ranged from 0.84 to 1.14.
Accuracy Archived	The median dark current was 0.0041 electron/s/pix both early in the cycle, with side-1 electronics, and after the recovery, with side-2 electronics. Signal to noise for the median count rate, for a combination of about 56 exposures of 1100 s each in the baseline dark, was 7 for the side-1 electronics and 6 for the noisier side-2 electronics.
Continuation Plans	Continued without change in Cycle 10 programs 8901 and 8902.

Figure 1: Histogram of intensities (electrons/s/pixel) for a dark reference file made for a week in August 2001 using side-2 electronics.



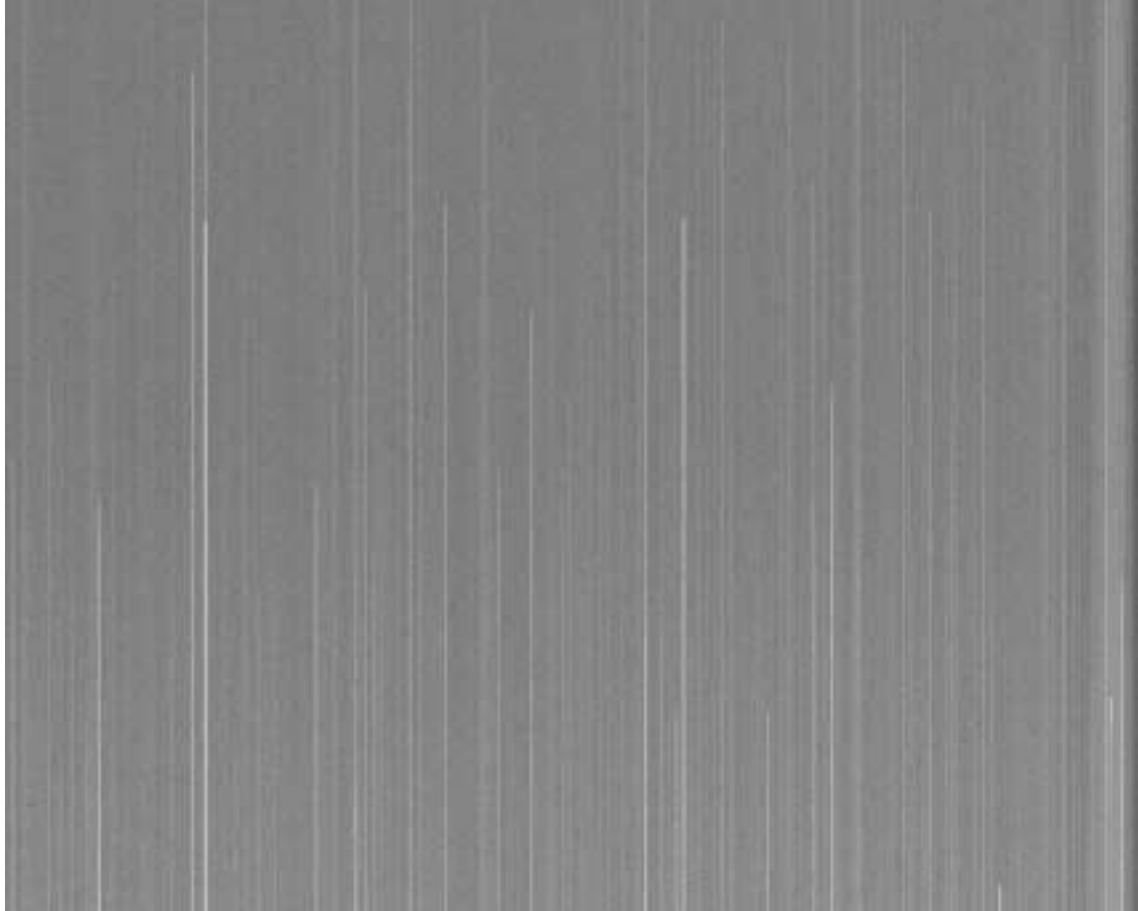
Proposal ID 8838 & 8865: CCD Bias Monitor

Execution	Executed once per day (8838 in the first half of the cycle, 8865 in the second half) except for the period when STIS was safed (May 16 - Jul 11, 2001).
Summary of Goals	Produce bias reference files for gain 1 unbinned (weekly files) and gain 1 binned 1x2, 2x1, 2x2 (biweekly files) and gain 4 unbinned (biweekly files). Achieve signal to noise good enough to measure hot columns on these time scales.
Summary of Analysis	Bias file production is described in ISR 99-08 and TIR 2000-05 . Data taken between monthly anneals is combined weekly (gain 1 unbinned) or biweekly to produce bias reference files. If a weekly or biweekly time period is short of data, the data from that time period are used to update hot columns in a baseline bias image, made from all data taken during that anneal period. This combination thus provides good signal-to-noise in normal columns while updating hot columns.
Accuracy Archived	This program was designed to achieve a signal-to-noise of at least 1 per pixel for each bias reference file. The achieved S/N is given in Table 4 for data taken early in the cycle with side-1 electronics and data taken late in the cycle with side-2 electronics. Pattern noise in the gain=1 data taken with side-2 electronics has somewhat degraded the S/N of the reference files. (Gain=4 data has always had significant pattern noise.)
Continuation Plans	Continued without change in Cycle 10 programs 8903, 8904.

Table 4. Median bias level, read noise, and signal-to-noise for bias reference files at the beginning of Cycle 9 (with side-1 electronics; first entry) and after 11 Jul 2001 (with side-2 electronics; second entry)

Gain	Binning	Median (ADU)	Read noise per exposure (ADU)	Number of exposures combined	Read noise in ref file (ADU)	S/N per pixel in ref file
1	1x1	0.75	4.3	98	0.43	1.7
		0.67	5.7	98	0.58	1.2
1	1x2	1.14	4.3	28	0.81	1.4
		0.82	5.6	28	1.06	0.8
1	2x1	1.06	3.9	28	0.74	1.4
		1.07	4.7	28	0.89	1.2
1	2x2	1.55	3.9	28	0.74	2.1
		1.57	4.8	28	0.91	1.7
4	1x1	1.65	1.9	42	0.29	5.7
		1.64	1.9	42	0.29	5.7

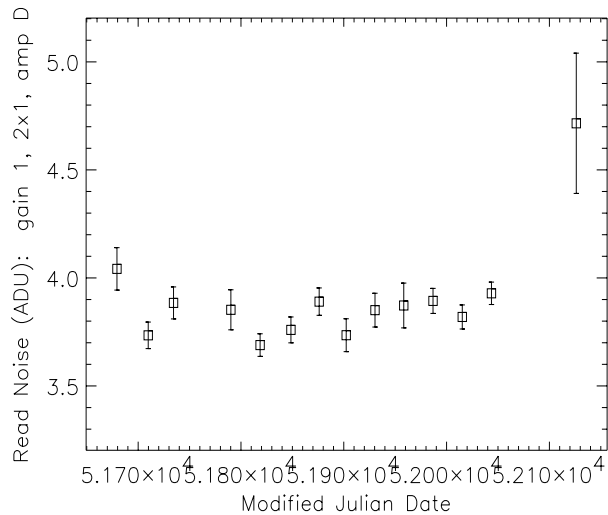
Figure 2: Unbinned gain 1 bias reference file (side-2 electronics) for one week in August, 2001. The display saturates at 6.5 ADU/pixel.



Proposal ID 8840: CCD Read Noise Monitor

Execution	Executed once per month from July 2000 to August 2001 except for three months, including two months during the period when STIS was safed (summer 2001).
Summary of Goals	Monitor the read noise in all amplifiers (A,B,C,D) for gain=1 and gain=4 and binnings 1x1, 1x2, 2x1, and 2x2.
Summary of Analysis	Pairs of bias frames were used to measure the read noise by measuring the rms dispersion in a difference image cleaned of discordant pixels via iterative sigma clipping. Batch mode programs were developed to make the measurements and produce cumulative tables and plots for the STIS calibration monitor web page each month. An example plot is shown in Figure 3. The read noise remained relatively stable from the initial measurements in May 2000 (program 8798) until the failure of the side-1 electronics in May 2001. The gain=1 read noise has been significantly higher for operations with the side-2 electronics, which began in July 2001. For example, the readnoise for the commonly used combination of amplifier D, gain=1, binning 1x1 increased from 4.5 electrons to 5.4 electrons. The read noise has always been larger for gain=4 than for gain=1, and remains at 7.5 electrons for amplifier D, binning 1x1.
Accuracy Archived	Typical errors in the read noise measurements are +/-0.05 DN through May 2001. The errors are larger in the last gain 1 data taken in August (~0.3 DN) because of the pattern noise generated by the side-2 electronics. (Gain=4 has always had substantial pattern noise, which is not significantly different for side-2 operations.)
Continuation Plans	Continued without change in Cycle 10 program 8905.

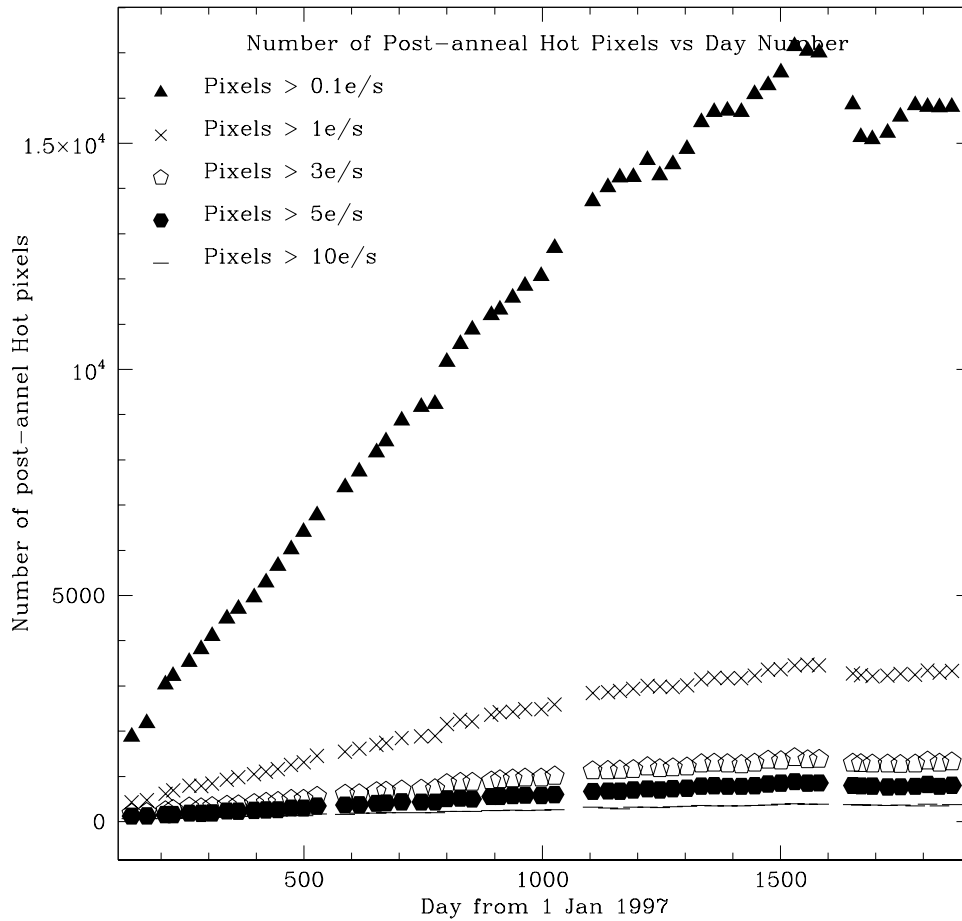
Figure 3: Monthly read noise measurements for gain=1, binning 2x1, amplifier D, commonly used for spectral imaging of faint targets. The last data point is for side-2 electronics.



Proposal ID 8841: CCD Hot Pixel Annealing

Execution	Groups of three visits executed approximately once every four weeks between September 2000 and August 2001. The first visit in each group consisted of pre-anneal darks and flats, the second contained a special command to turn off the CCD cooler for the period of the anneal, and the third visit contained the post-anneal darks and flats. The group of three visits that was to have occurred in June 2001 did not execute because of the STIS side-1 failure, and these visits were not rescheduled.
Summary of Goals	Anneal the STIS CCD and monitor the effectiveness of the anneal by taking pre- and post-anneal dark images.
Summary of Analysis	<p>Reports and figures summarizing the anneal results are posted monthly on the STIS monitors page, http://www.stsci.edu/hst/stis/calibration/monitors/. Since the side-2 electronics do not contain a working temperature control circuit for the CCD, after June 2001, the CCD could no longer be operated at a fixed temperature. As the dark current in each hot pixel is temperature dependent, it was necessary to scale the side-2 darks to a common temperature before computing the statistics of the anneal. This is done using the CCD housing temperature (header keyword OCCDHTAV) as a surrogate for the CCD temperature. A dependence of 7% per degree C was found (T. Brown, STIS ISR 2001-003). The darks are scaled to a housing temperature of 18 C. This apparently corresponds to an actual CCD chip temperature somewhat lower than the side-1 operating temperature of -83 C. As a result side-1 and side-2 dark rates and hot pixel levels are not directly comparable to each other. However, the statistics should accurately reflect the mean side-2 dark current.</p> <p>After the 1 May 2001 anneal, the last prior to the side-1 failure, there were 17012 hot pixels at > 0.1 e/s level, 3455 at > 1.0 e/s, and 389 with > 10 e/s. After rescaling them to OCCDHTAV=18 C, the July 2001 post-anneal side-2 darks had 15866 pixels with > 0.1 e/s, 3278 > 1.0 e/s, and 379 > 10 e/s. The decrease is due, not to a real decrease in the number of hot pixels, but to a decreased dark current in each hot pixel. The post-anneal darks on 21 August, showed similar results, with 15093 > 0.1 e/s, 3215 > 1.0, and 363 > 10 e/s. The mean dark rate during side-1 operations was 0.0042 cts/sec/pixel, and 0.0038 cts/sec/pixel during side-2.</p>
Accuracy Archived	During the period of side-1 STIS operations covered by this proposal between September 2000 and May 2001, the monthly anneals healed an average of 89+/-23 percent of the new hot pixels (>0.1 e/s) created each month.
Continuation Plans	Continued in Cycle 10 program 8906.

Figure 4: The number of hot pixels found shortly after each monthly anneal of the CCD is shown as a function of time. This figure includes data from several cycles of anneal monitors. Side-2 darks are scaled to 18 C before the statistics are computed.



Proposal ID 8845: CCD Spectroscopic Flats

Execution Visits 61, 62, 63, 66, 67, 68, 69, 70, and 71 failed because the STIS side-1 electronics malfunctioned shortly before they were scheduled to execute. These visits were not rescheduled. Visit 31, 34, and 9A were also withdrawn because of the STIS side-1 electronics failure.

The SLIT-STEP optional parameter was used in this program to move the aperture bars to different locations on the detectors. However, a new SLIT-STEP value only takes effect if the aperture differs from the aperture used in the previous exposure line. A failure to understand this behavior resulted in many exposures being executed with different aperture positioning than desired. However, this error did not seriously compromise the objectives of this program.

Otherwise, all visits executed as expected.

Summary of Goals The STIS CCDs have very small pixel-to-pixel variations, with a typical RMS scatter of about 1% outside of the dust motes. Using a pflat file makes a significant difference only for very high S/N observations, but for such observations it is important that the pflat be of very high S/N itself; otherwise its use may give worse results than no pflat at all. This program combines deep monthly lamp flats using G430M to monitor the overall variations in the pflat, along with annual checks of each of the individual gratings to verify the uniformity of the pflat across gratings.

Summary of Analysis It has been shown (see **STIS ISR 99-06**) that the CCD pflat is independent of wavelength, except that the shape and location of the dust motes differ slightly between the L and M modes due to the anamorphic magnification. The pflat does, however, change significantly with time. So the bulk of our analysis concentrated on the G430M observations, as these are the most numerous. A new pflat was constructed using these G430M lamp exposures. For the L mode gratings the data near the dust motes were replaced with the values in the previous Cycle 7 pflat, as these are of higher S/N than the available data from this program. After excluding the dust motes, the rms residuals of the ratio of the new pflat and the old pflat based on Cycle 7 data is about 0.5%.

The new pflat was tested using coadded G750L spectra of the standard stars GD71 and G191, divided by the theoretical spectrum for each of these stars. At the short wavelength end of the G750L spectrum, where the IR fringing is unimportant and the S/N highest, use of the new pflat reduces the rms residuals from 0.37% to 0.33% for the GD71 data, and from 0.35% to 0.29% for the G191 data.

Since the new pflat does give improved results for data taken during Cycle 9, new pfl reference files for all CCD spectroscopic modes were prepared and delivered for pipeline use.

Accuracy Archived RMS residuals at least as small as 0.3% can be obtained with sufficiently deep spectroscopic observations.

Continuation Plans Continued in Cycle 10 program 8907.

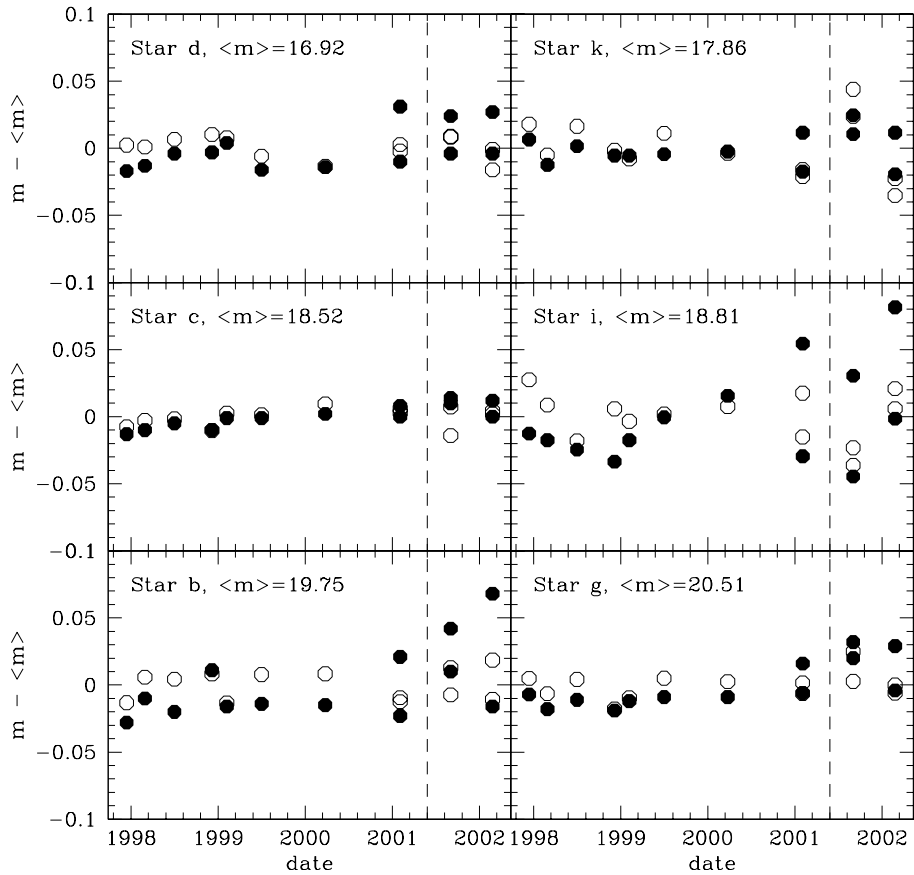
Proposal ID 8846: CCD Imaging Flats

Execution	Two visits that were scheduled to have occurred while STIS was inoperative due to the side-1 electronics failure were withdrawn. Otherwise, all visits executed as planned.
Summary of Goals	The STIS CCDs have very small pixel-to-pixel variations, with a typical RMS scatter of about 1% outside of the dust motes. This program obtained a series of imaging CCD flats every month to monitor the characteristics of the CCD pixel-to-pixel response, and to look for the development of new cosmetic defects.
Summary of Analysis	The combined 50CCD monitor observations from this program were compared with the pre-launch imaging pflat currently used in the pipeline. After correcting for the expected Poisson errors, the residual RMS difference between the monitor observations and the reference pflat are about 0.35%. Visual comparison of the monitor data with the reference pflat showed no significant new cosmetic defects.
Accuracy Archived	RMS differences from previous pflat are about 0.35%.
Continuation Plans	Continued in Cycle 10 program 8908.

Proposal ID 8847: CCD Full-Field Sensitivity Monitor

Execution	Visits successfully completed in Sep 2000 and Feb 2001.
Summary of Goals	A photometric standard star field in Omega Cen is measured with the unfiltered STIS 50CCD mode every six months to monitor CCD sensitivity over the whole field of view. To keep the same stars in the same part of the CCD for every measurement, the spacecraft orientation is kept within a suitable range (+/- 5 deg). The second observation is taken at an orientation rotated by 180 degrees with respect to the other observation. Since 2001, observations were taken with both long and short exposures to test for CTE effect.
Summary of Analysis	The data were combined with similar data obtained in previous cycles. This included observations taken after the STIS safing in July 2001 and the subsequent recovery using the side-2 electronics. A set of stars of different magnitudes and at different positions on the detector were selected, and aperture photometry was carried out for these stars at different epochs. The data taken over the past four years were analyzed.
Accuracy Archived	(a) for stars of different brightnesses, changes in their magnitudes (defined as the difference between the observed and mean magnitude) is < 1% a year over the past four years. (b) No changes in the throughput are found after the switch to the STIS side-2 electronics. (c) For any given epoch, the difference between magnitudes from long and short exposures increases for fainter stars. The change is from 0.01 (at m=16.93) to 0.07 (at m=20.56). The observed difference is due to CTE effect. Once corrected for CTE effect, this difference in magnitude of stars in long and short exposures decreases to the level of poisson noise. The CTE correction also tightens up the overall scatter around the mean magnitude for a given star over all epochs and positions on the detector. (d) For stars of a given color, a change in full-field sensitivity of < 1% is found.
Continuation Plans	Continued in Cycle 10 program 8912.

Figure 5: The difference between the mean magnitude and the magnitude at a specific epoch of a given star (at a different position on the CCD) over time. Each panel is for a given star at a given magnitude as indicated. Filled circles show the raw data; open circles show the magnitudes corrected for CTE. The vertical, dotted line in each panel corresponds to the switch to the side-2 electronics. The last three epochs show two measurements for each epoch. One measurement is from long (60 sec) exposures and one is from short (10 sec) exposures. As can be seen, the CTE correction reduces the difference between these long and short exposures.



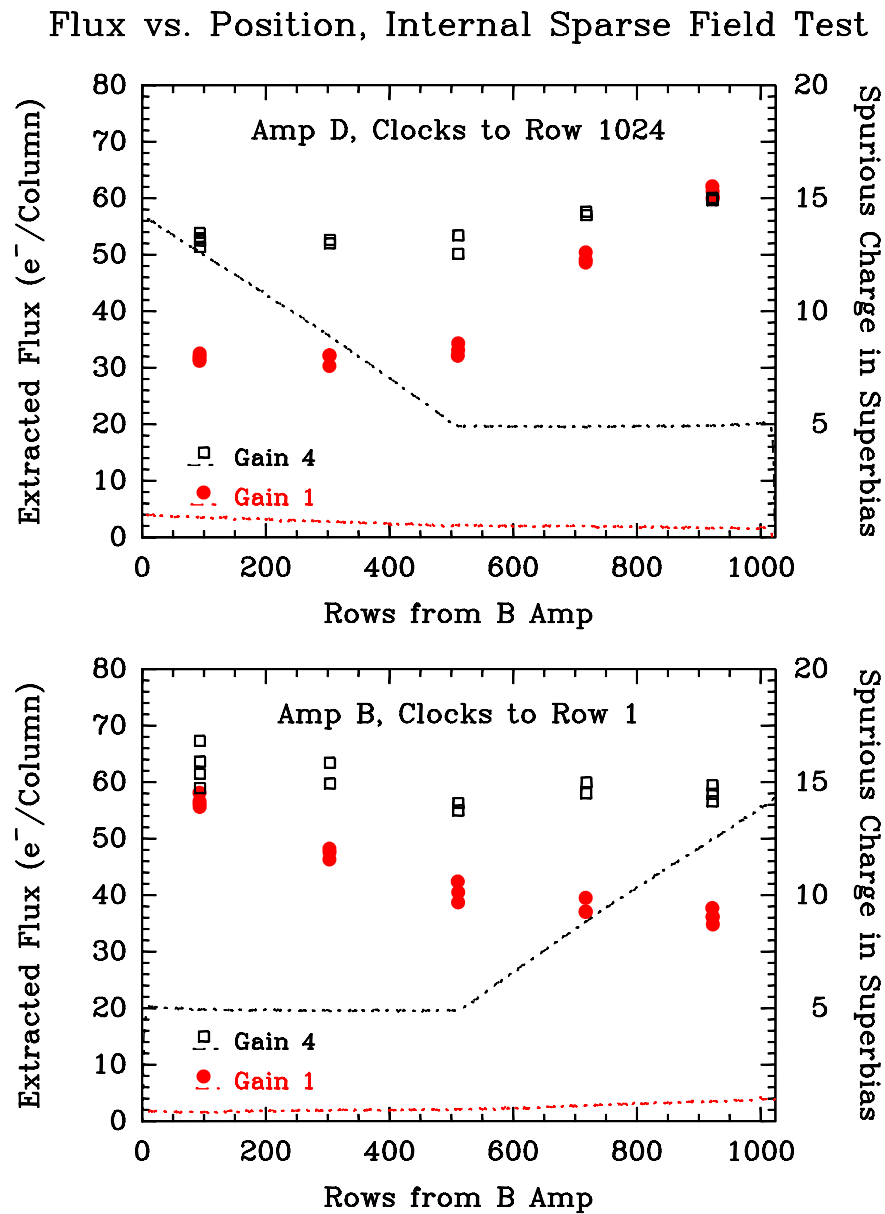
Proposal ID 8848: CCD Dispersion Solutions

Execution	The four visits of this program executed successfully between 4 September and 8 September, 2000.
Summary of Goals	Obtain deep engineering wavecalcs for all CCD gratings at several wavelength centers as a yearly monitor of derived dispersion solutions.
Summary of Analysis	<p>Since this program completed execution, we have implemented the new E1 pseudo-aperture positions, which place the spectrum near row 900 in order to mitigate CTE effects for faint spectra. Preliminary analysis of the 8848 data shows that these internal wavecalcs, which used the standard LINE lamp, are not deep enough to determine the dispersion relation near row 900 where the new E1 apertures are defined. The illumination pattern of this lamp simply does not reach high enough on the detector.</p> <p>Because of the importance of the new E1 aperture locations, lamp exposures using the HITM1 lamp, which provides better illumination near row 900, were done for all CCD gratings in the Cycle 11 calibration program 9617. For these reasons, final revision of the CCD wavelength calibration will be deferred until the new Cycle 11 data can be analyzed.</p>
Accuracy Archived	N/A
Continuation Plans	Continued as Cycle 10 program 8909.

Proposal ID 8851: CCD Sparse-Field CTE internal

Execution	Visits 1A - 25 (32 visits, CCD Gain = 1) executed successfully during Oct 26-31, 2000; Visits 3A - 45 (32 visits, CCD Gain = 4) executed successfully during Apr 1-9, 2001.
Summary of Goals	Measure Charge Transfer Efficiency (CTE) for point-like sources in a sparse field along the parallel register, as a function of source intensity. Use bi-directional clocking method.
Summary of Analysis	<p>A sequence of nominally identical exposures is taken, alternating the read-out between amplifiers on opposite sides of the CCD. After correcting for gain differences in the read-out chains, the observed ratio of the fluxes seen by the two amplifiers can be fit to a simple model of constant fractional charge loss per pixel transfer. By fitting the observed flux ratio at a range of source positions along the columns, one can confirm that what is being measured is indeed a charge transfer effect. This "internal" version of the "sparse field test" is as follows. Using an on-board tungsten lamp, the images of a narrow slit is projected at five positions along the CCD columns. The data from this program are representative of "worst-case" spectroscopic observations, because there is essentially no sky background to provide any filling of charge traps in the image array. At each position, the alternating sequence of exposures mentioned above is taken. For each exposure, the average flux per column within a standard 7-row extraction aperture and the centroid of the image profile within those 7 rows is calculated. The alternating exposure sequence allows CTE effects to be separated from warm-up effects of the calibration lamp.</p> <p>Derived CTI (Charge Transfer Inefficiency) values have been shown to increase as a function of on-orbit time. The CTI is also found to decrease with increasing signal level. Detailed analysis of the internal CTE monitoring data, including data from proposal 8851, is described and illustrated in Kimble, Goudfrooij & Gilliland (2001, SPIE 4013, 532). Here we show a different result of the internal CTE monitor data, namely one showing the relatively strong effect of the local background level for low-intensity sources. Figure 6 shows a clear anticorrelation between the charge loss (i.e., CTI) and the local background level. Note that in this case, the background is due to spurious charge present in superbias frames; the GAIN=1 and GAIN=4 settings have different levels of spurious charge (which results from a difference in bias voltages between the two gain settings).</p>
Accuracy Archived	CTI values are accurate to within 1% for signal levels > 200 electrons per extraction at the center of the CCD.
Continuation Plans	Continued in Cycle 10 proposal 8910.

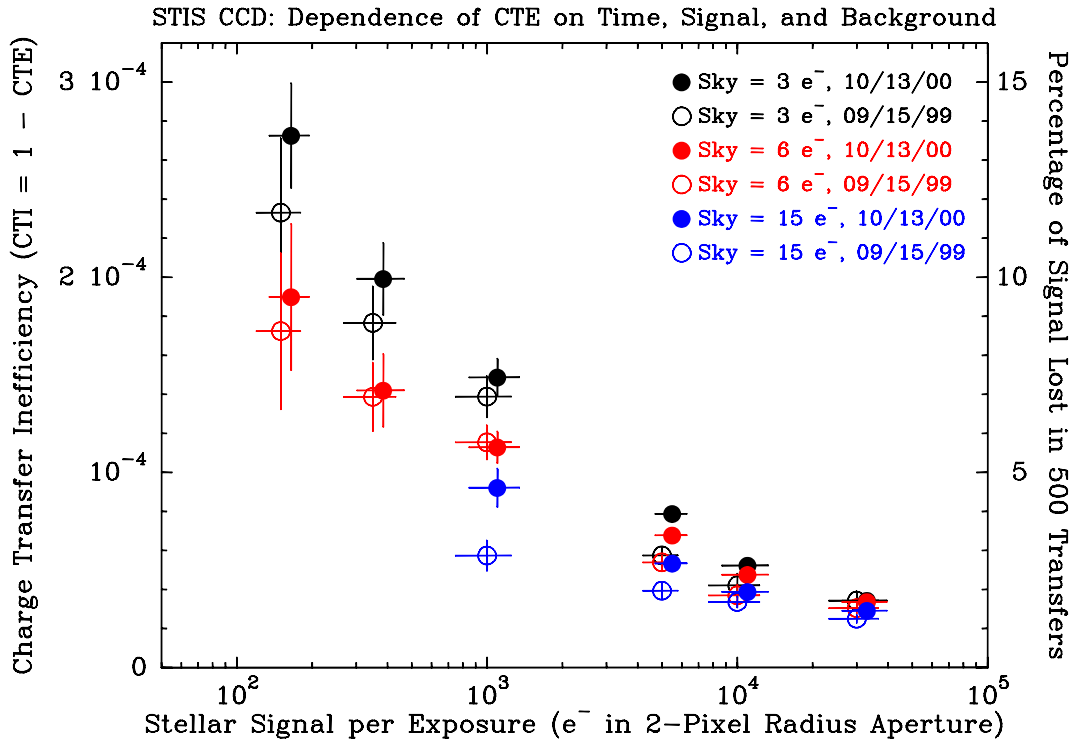
Figure 6: An illustration of the effect of local background level to the charge loss for low-intensity sources. Top panel shows results for D-amp readout, bottom panel for B-amp readout. In both panels, the symbols show the average flux per column within a standard 7-row extraction aperture (levels indicated on left-hand ordinate; see summary of analysis above) as a function of position along the parallel register (or the Y coordinate in regular STIS images). The superimposed dot-dashed lines show the background (unit is electrons; levels are indicated on right-hand ordinate) from spurious charge (created during read-out, present in superbias files) in the two supported gain settings (GAIN=1 in red, GAIN=4 in black). Note the clear anticorrelation between charge loss and local background level.



Proposal ID 8854: CCD Sparse-Field CTE external

Execution	Visit 1 executed successfully during UT October 13, 2000. Visit 2 executed successfully during UT September 27-28, 2000.
Summary of Goals	Measure Charge Transfer Efficiency (CTE) for point sources in a sparse field along the parallel register, as a function of source intensity and (local) sky background. Use bi-directional clocking method.
Summary of Analysis	<p>A sequence of nominally identical exposures is taken, alternating the read-out between amplifiers on opposite sides of the CCD. After correcting for gain differences in the read-out chains, the observed ratio of the fluxes seen by the two amplifiers can be fit to a simple model of constant fractional charge loss per pixel transfer. By fitting the observed flux ratio at a range of source positions along the columns, one can confirm that what is being measured is indeed a charge transfer effect.</p> <p>This “external” version of the “sparse field test” is as follows. Imaging exposures are taken at an off-center position in globular cluster NGC 6752 which is located in the CVZ. Exposures of 20s, 100s and 500s are cycled through on the same field containing several hundred stars with a wide range of intrinsic brightness. By cycling through the exposures over a full CVZ orbit we can be assured of encountering high sky levels for as large a subset of exposures as possible. This imaging is done using the clear filter.</p> <p>Slitless spectroscopy exposures with G430L are taken of a field in open cluster NGC 346. The visit consists of 3 CVZ orbits in which exposures of 20s, 100s, and 500s are cycled through on the same field containing ~50-100 stars with a wide range of inherent brightness. Again, the CVZ provides variable background. Each of the above visits uses the standard science observing mode; a near-copy of each orbit is included using the CCD amplifier on the opposite side of the detector (B) in order to determine the CTE.</p> <p>For appropriate stars in the field, fluxes are extracted within a range of extraction apertures, and the local background is also measured. The DAO-PHOT-II package is used for the imaging exposures. For the slitless spectroscopy exposures, fluxes are extracted for three regions along the dispersion direction which have distinct background levels (due to the influence of the three strong emission lines [OII]3727, Hbeta, and [OIII]5007). The standard 7-pixel aperture is used to extract fluxes.</p> <p>Derived CTI (Charge Transfer Inefficiency) values have been shown to increase as a function of on-orbit time. The CTI is also found to decrease with increasing signal level, as well as with increasing background level. Detailed analysis of the CTE monitoring data, including data from proposal 8854, is described and illustrated in Kimble, Goudfrooij & Gilliland (2001, SPIE 4013, 532). Quantitative results on the CTI from proposal 8854, including updates on the time dependence of the CTE as a function of source intensity and sky background, were published in Chapter 7 of the STIS Instrument Handbook v5.1 (in particular Table 7.4). Figure 7 illustrates the evolution of the CTI as a function of source intensity and sky background.</p>
Accuracy Archived	CTI values are accurate to within 1% for signal levels > 200 electrons per extraction at the center of the CCD.
Continuation Plans	Continued as Cycle 10 proposal 8911.

Figure 7: Parallel CTI (and percent charge loss from CCD row #500) for point sources, derived from the external sparse field test (proposal 8854). Note the significant effect of even a modest background level (e.g., 15 electrons/pix). Results are plotted for two epochs: 2.45 and 3.6 years after launch (see legend at top right). The data for two epochs are plotted at slightly different signal levels for clarity. The CTI is found to increase by ~15% per year on average.



Proposal ID 8855: Slit Wheel Repeatability

Execution	Executed on Feb 8, 2001.
Summary of Goals	Check the stability of the STIS slit wheel from a sequence of comparison lamp spectra using the grating G230MB (centered at 2697 Å) and the three smallest long slits (52X0.2, 52X0.1, and 52X0.05).
Summary of Analysis	A total of 24 measurements over a 40 minute period were obtained with the LINE lamp to check the repeatability of the slit wheel. The data were processed with the WAVECAL task, which compares the observed lamp spectra with the template wavecal. For Cycle 9, the AXIS1 data seem to follow a trend that we attribute to thermal variations in the spacecraft. A 3rd order fit of this trend was made for each aperture and subtracted from the data. The resulting average dispersion about this fit is 0.006 pixels (0.3 milli-arcsec). A weak linear trend is also seen in the AXIS2 data, which is the direction of motion of the slit wheel. After subtraction, the spatial direction (AXIS2) shows an average dispersion of 0.022 pixels (1.1 milli-arcsec). Applying this same analysis to the Cycle 8 data, we found that there is no significant degradation of the slit wheel repeatability.
Accuracy Archived	The slit wheel is repeatable to an accuracy of 0.022 pixels or 1.1 milli-arcseconds.
Continuation Plans	Continued in Cycle 10 program 8913.

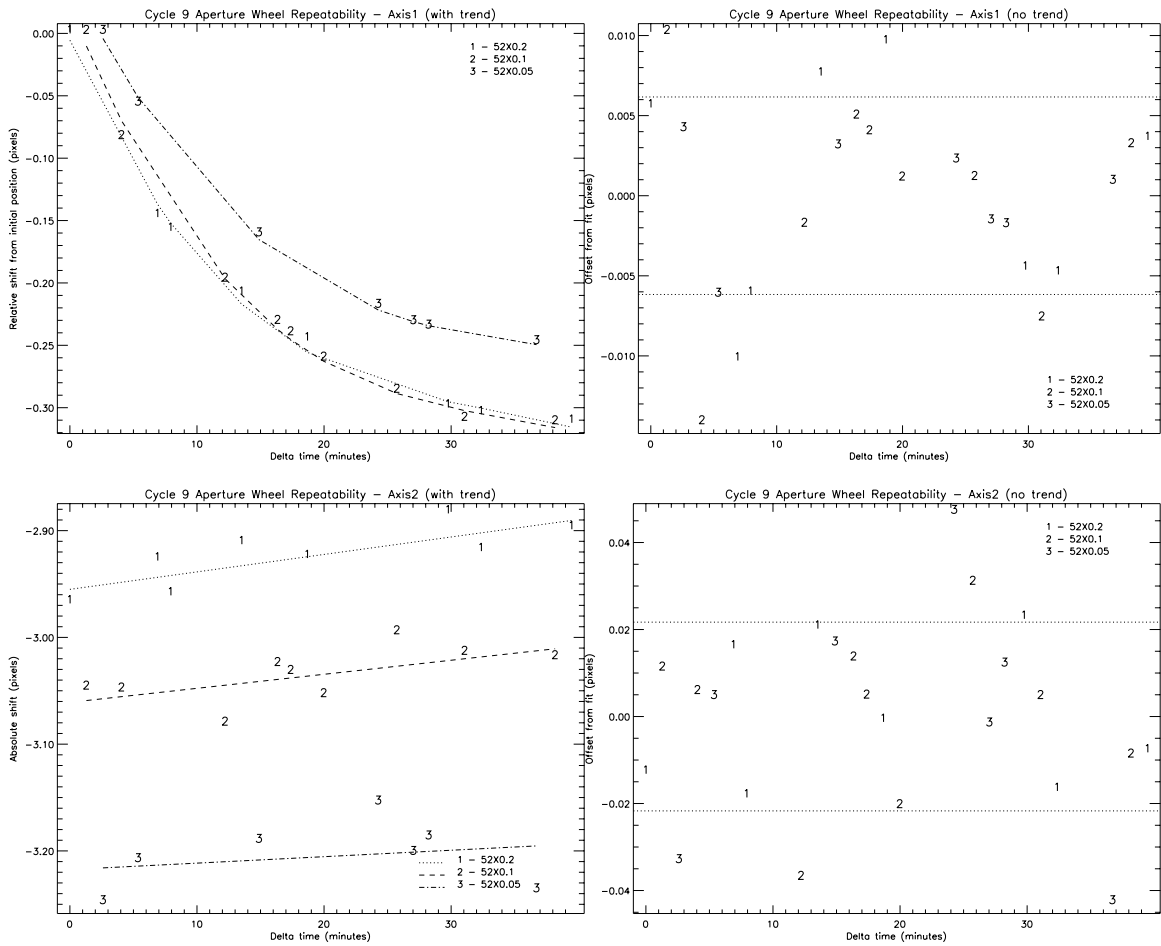
Table 5. Slit wheel repeatability measurements.

Dataset name	Aperture	Delta time (minutes)	Absolute shift (pixels)		Relative shift (pixels)	
			Axis1	Axis2	Axis1	Axis2
o68l01k0q	52X0.05	2.600	-0.641	-3.750	0.000	0.000
o68l01k2q	52X0.05	5.367	-0.698	-3.710	-0.058	0.039
o68l01k8q	52X0.05	14.883	-0.803	-3.692	-0.162	0.057
o68l01keq	52X0.05	24.267	-0.861	-3.656	-0.220	0.093
o68l01kgq	52X0.05	27.033	-0.874	-3.703	-0.233	0.046
o68l01khq	52X0.05	28.233	-0.877	-3.689	-0.236	0.061
o68l01kmq	52X0.05	36.717	-0.890	-3.738	-0.249	0.011
o68l01jzq	52X0.1	1.300	-0.543	-3.048	0.000	0.000
o68l01k1q	52X0.1	4.067	-0.628	-3.050	-0.084	-0.002
o68l01k6q	52X0.1	12.217	-0.742	-3.082	-0.199	-0.034
o68l01k9q	52X0.1	16.350	-0.776	-3.026	-0.232	0.022
o68l01kaq	52X0.1	17.383	-0.785	-3.034	-0.242	0.015
o68l01kcq	52X0.1	19.983	-0.805	-3.056	-0.262	-0.007
o68l01kfq	52X0.1	25.733	-0.831	-2.997	-0.288	0.052
o68l01kjq	52X0.1	31.067	-0.854	-3.016	-0.310	0.033
o68l01knq	52X0.1	38.183	-0.856	-3.020	-0.313	0.028
o68l01jyq	52X0.2	0.000	-0.778	-2.968	0.000	0.000
o68l01k3q	52X0.2	6.900	-0.926	-2.928	-0.147	0.040
o68l01k4q	52X0.2	7.933	-0.937	-2.961	-0.158	0.008
o68l01k7q	52X0.2	13.517	-0.988	-2.913	-0.209	0.055
o68l01kbq	52X0.2	18.683	-1.024	-2.926	-0.246	0.042
o68l01kiq	52X0.2	29.767	-1.078	-2.884	-0.300	0.084
o68l01kkq	52X0.2	32.367	-1.084	-2.919	-0.305	0.049
o68l01koq	52X0.2	39.483	-1.090	-2.899	-0.312	0.069

Table 6. Annual measurements of the slit wheel repeatability.

Cycle	Date	Dispersion direction	Spatial direction
8	Jan 12 2000	0.005 pix (0.3 milli-arcsec)	0.016 pix (0.8 milli-arcsec)
9	Feb 08 2001	0.006 pix (0.3 milli-arcsec)	0.022 pix (1.1 milli-arcsec)

Figure 8: Distribution of slit wheel positions before and after thermal trend removal.



Proposal ID 8856: CCD Sensitivity Monitor

Execution	Executed as planned from October 2000 to August 2001. 1 orbit every 3 months for the L modes and 1 orbit every 6 months for the M modes, for a total of 6 orbits.
Summary of Goals	Monitor the sensitivity of each CCD grating mode to detect any change due to contamination or other causes.
Summary of Analysis	Cumulative analysis of new data is maintained by David Stys. Previous trends continue. The observed trends in the CCD modes are dominated by CTE loss. The rates of sensitivity loss (including CTE loss) for the CCD L-modes range from ~0%/yr (G750L) to ~2%/yr (G230LB), while the M-mode sensitivity losses range from ~1%/yr (G750M) to ~4%/yr (G230MB). Due to lower exposure levels, the CCD M-mode exposures experience significantly larger CTE losses than in the L-modes. A new ISR has been written and will be published upon review.
Accuracy Archived	The rms scatter is consistent with previous cycles, while the accuracy of the trend fits is higher due to the increasing temporal baseline (see ISR STIS 2001-01R).
Continuation Plans	Continued in Cycle 10 program 8914.

Proposal ID 8842: CCD PSF Library

Execution	All visits executed successfully between July and September 2000.
Summary of Goals	<p>This program obtained high S/N observations (both saturated and unsaturated) of an A and an F star. These observations were intended to provide deep subsampled F28X50LP and 50CCD images for the STIS PSF library, and to place better constraints on the CCD imaging absolute throughput as a function of wavelength. This was necessary because of apparent discrepancies in the previously adopted long wavelength CCD throughput. G750L spectra of these two stars were also taken to measure their intrinsic flux distribution. Coronagraphic observations of HD154363 (K5V, B-V = 1.10) were also included in this program to fill out the color range of standard Coronagraphic observations at the WEDGEA1.0 and WEDGEA1.8 positions.</p>
Summary of Analysis	<p>These observations were used in conjunction with data from the Cycle 8 CAL/STIS program 8422 to check and revise the red-end sensitivity of STIS/CCD imaging modes. A new CCD imaging throughput curve was derived and the corresponding reference files for the STIS pipeline and SYNPHOT calculations were delivered to CDBS. An ISR describing the analysis, the throughput changes, and recommended aperture corrections for STIS/CCD imaging observations is nearly complete, and will be submitted shortly.</p> <p>The deep dithered images obtained during this program have also been coadded to produce deep subsampled PSF images.</p> <p>The Coronagraphic observations of HD154363 have been included by Carol Grady in a paper on the STIS Coronagraphic PSF, that is also expected to be completed shortly and submitted for publication in the PASP.</p>
Accuracy Archived	We estimate that the revised CCD flux calibration should be good to about 3%.
Continuation Plans	Cycle 10 program 8924 "CCD PSF and LP Filter Curve Calibration" obtained additional images and spectra of the F star CPD-60D7585 = SAO255271, as well as of a K dwarf. This additional data will be used to verify the new CCD imaging throughput curve, as well as to expand the range of colors for which empirical aperture corrections are available.

Proposal ID 8844: Deep Spatial/Spectral PSF Calibration

Execution The four visits of this program executed in July and August of 2000. All observations executed as planned. During visit three the target was just outside the initial acquisition image, but the fine locate phase seems to have nevertheless successfully acquired the target, and no impact on the calibration goals of this program is anticipated.

Summary of Goals The primary purpose of this program was to acquire, with the STIS CCD, a set of deep spectroscopic images of isolated point source stars for the purpose of correcting spectroscopic science observations for the dispersed residual scattered light along the slit. The hope is to achieve a useful dynamic range of as much as 10^7 for the study of circumstellar material up to 26" away from a point source target.

Summary of Analysis The data analysis is being undertaken by the IDT at GSFC including Ted Gull (NASA/GSFC), Don Lindler (ACS/GSFC), and Don Tennant (USNA). Work is still ongoing, and only preliminary results are reported here.

Several problems have complicated the data analysis, including problems with the bias subtraction, window ghosts, and other asymmetries in the cross dispersion point spread function. While the diffraction pattern can easily be modeled and subtracted as a function of wavelength, scattered light due to micro-roughness of the mirror surface and scattering within the detector chip or supporting glass is far more difficult to model and correct.

Analysis so far has focused on a relatively clean region 20 rows wide 50-70 rows above the stellar spectrum. Between 2000 to 5500 Å the flux through the 52X0.2 aperture (summed over this 20 row wide strip) is about 0.005 of the total stellar flux. This fraction increases to 0.028 at 9750 Å. With the star is placed behind the F1 or F2 fiducial, the fractional light in the test strip drops to about 0.00003 between 3000 to 6500 Å, while below 3000 Å the fractional light climbs to nearly 0.00006. Longward of 6500 Å, the fractional light increases substantially for the fiducials reaching 0.00027 (~1% of the 52X0.2 aperture flux) at 9750 Å for 52X0.2F1 and 0.00011 for the 52X0.2F2 aperture. Results for most G430M and G750M settings are consistent with the L mode results. An exception is the 8825 Å setting of the G750M; for this grating, the fractional light between 8200 to 9000 Å appears to be 50% higher than in the G750L. Note that the flux levels quoted here are the fraction in these 20 rows.

Accuracy Archived Still under evaluation.

Continuation Plans None

Proposal ID 8850: Deep CCD/G750M Wavecals

Execution	All visits executed on July 12 and 13, 2000.
Summary of Goals	This program was intended to provide deep on-orbit wavecals for long wavelength settings of the G750M, in order to improve the dispersion relation for these modes, and to provide significantly better than the then achievable 1 pixel wavelength accuracy.
Summary of Analysis	<p>Since this program executed we have implemented the new E1 pseudo-aperture positions, which place the spectrum near row 900 in order to mitigate CTE effects for faint spectra. Preliminary analysis of the 8850 data showed that these internal wavecals, which used the standard LINE lamp, are not deep enough to determine the dispersion relation near row 900 where the new E1 apertures are defined. The illumination pattern of this lamp simply does not reach high enough on the detector.</p> <p>Because of the importance of the new E1 aperture locations, lamp exposures using the HITM lamp, which provides better illumination near row 900, were added to the Cycle 11 calibration program 9617. In the meantime, the STIS IDT also developed and delivered to STScI an improved wavelength solution for on-axis G430M and G750M data, derived using observations of an external line source. For these reasons, final revision of the G750M wavelength calibration will be deferred until the new Cycle 11 data can be analyzed.</p>
Accuracy Archived	N/A
Continuation Plans	See Cycle 11 program 9617, STIS CCD Spectroscopic Dispersion Monitor

Proposal ID 8852: Measurement of CCD Window Ghost in Spectrographic Mode

Execution	Target observed Aug 16, 2000.
Summary of Goals	<p>Window ghosts in STIS CCD imaging mode have been extensively studied (see IDT Postlaunch Quicklook Report 63 by R. S. Hill). This program was designed to test the assumption that the ghosts seen in spectroscopic STIS/CCD configurations have the same character as those seen in STIS/CCD imaging configurations, and that models of the reflection ghosts that the STIS/IDT developed are directly applicable to spectroscopic observations of external targets.</p> <p>To do this, a bright region of the Orion Nebula near HD 30720 with strong H-alpha emission was observed using the 0.2x0.2 aperture with the G750M grating at the 6768 Angstrom wavelength setting. This produces a point-like image on the detector.</p> <p>A number of internal line lamp exposures using the 0.2X0.2 aperture with the G430M, G430L, G750M, and G750L gratings were also taken to study the window ghosts at different wavelengths.</p>
Summary of Analysis	<p>Examination of the H-alpha image of the Orion nebula shows that this strong emission line displays a ghost very similar to that seen in imaging mode. The IDT procedure for modeling these ghosts was applied to this image and subtracting this model from the observed data was successful in removing this ghost.</p> <p>The ghosts seen in line-lamp images through the 0.2X0.2 aperture are significantly different from those produced by a narrow-lined sky source. They are less regular in shape and display prominent fringing. The lamp lines differ from the sky lines because they are narrower, they are not at infinity, and they are not obscured by the OTA secondary.</p> <p>Further details are given in IDT Postlaunch Quicklook Reports 63 and 65 by Robert S. Hill. These are available at http://hires.gsfc.nasa.gov/stis/postcal/quick_reports/quick_reports.html</p>
Accuracy Archived	The ghost was modeled and subtracted with better than 10% precision.
Continuation Plans	None

Proposal ID 8839: CTE for Extended Targets

Execution	Single visit for each of two targets.
Summary of Goals	Measure CTI as a function of signal level for extended sources, for application to science observations of galaxies.
Summary of Analysis	Spectral images were made of a nearby galaxy with a bright nucleus. The target was placed near the top of the CCD detector and readouts were made over a short distance (to amp D) and a long distance (to amp B). A range of signal strength was acquired by using the G430L grating and was further increased by using 3 different exposure times. Fluxes in the 7 spectral rows centered on the peak were measured across each image. Emission lines were clipped out to remove large gradients, then the fluxes in each image were reordered according to increasing strength in one of the longest exposures read out through the D amplifier (called the primary image). Flux ratios (B amp / D amp) were plotted against signal strength (exposure-time-scaled from the primary image), then medians were taken in 9 bins to improve signal to noise. An empirical correction was made for the apparent difference in the gain of the amplifiers. CTI was computed from flux ratio at each signal strength for each exposure time.
Accuracy Archived	The accuracy at each signal level can be deduced from the vertical scatter in the plots. For each exposure, the lower fluxes are generally at the bluer end of the spectrum. When flux ratios for different exposure times are plotted against signal strength, the shorter exposure flux ratios come from a redder part of the spectrum than the longer exposure flux ratios at a given signal strength. This appears to have a systematic effect on the flux ratios.
Continuation Plans	Continued in Cycle 10 program 8927, a similar spectroscopic program with the goal of measuring CTI effects on absorption line profiles in galaxies.

Figure 9: Flux ratio (B-amp readout / D-amp readout) versus signal in 7 spectral rows (electrons) for spectral images of a galaxy nucleus. Exposure times of 500s (asterisk), 305s (square), and 125s (triangle) are indicated. The signal on the x axis is exposure-time-scaled from the longest D amp exposure, so is essentially the signal without losses.

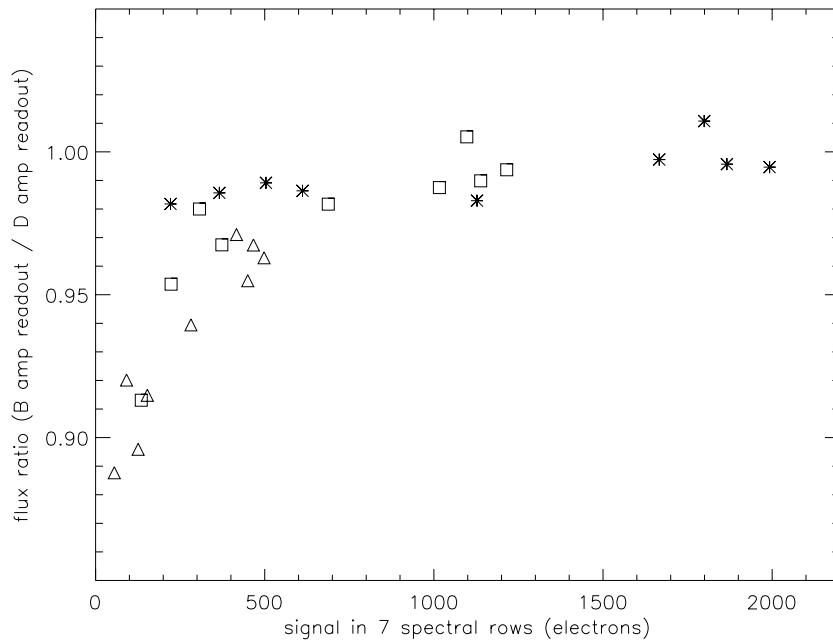
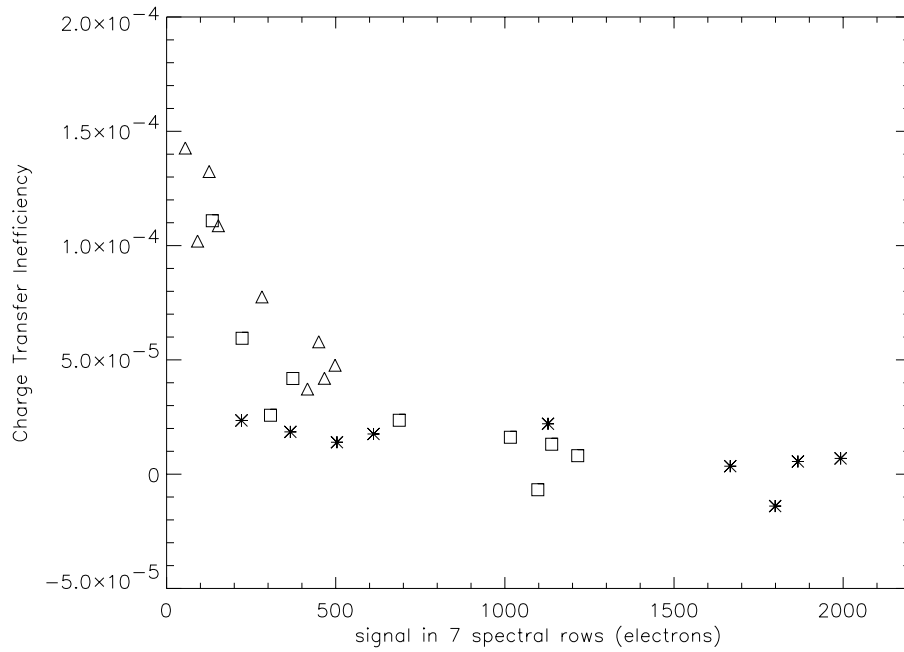


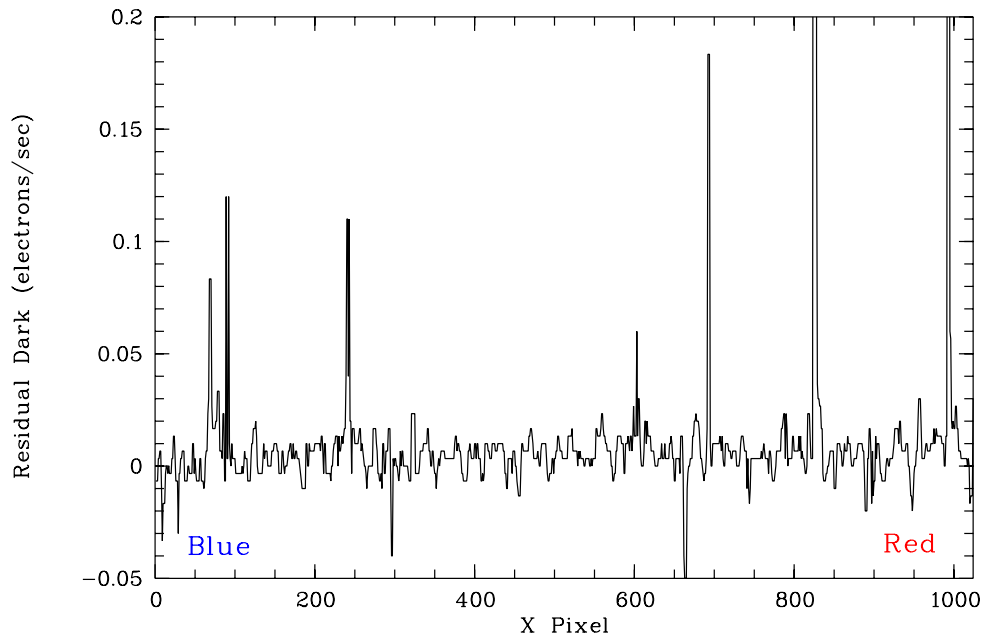
Figure 10: Charge Transfer Inefficiency versus signal in 7 spectral rows (electrons), computed from flux ratios (B-amp readout / D-amp readout). As before, exposure times of 500s (asterisk), 305s (square), and 125s (triangle) are indicated, and the signal on the x axis is exposure-time-scaled from the longest D-amp exposure.



Proposal ID 8853: CCD Residual Images after Overillumination

Execution	Executed on Aug 4-5, 2000.
Summary of Goals	Measure the residual effect of overillumination on the CCD as a function of source color (UV vs. Red).
Summary of Analysis	<p>The observational setup was as follows: Overexpose (by a factor of ~3) the CCD by taking a slitless spectrum of a bright star. Take three 5 min. dark frames afterwards to study the residual effect over time. Repeat the experiment, now taking bias frames instead of dark frames to study the effect of read-outs. Execute this procedure using two different settings, one in the UV (G230LB grating, using a blue star), and one in the red (using a tungsten lamp with a neutral density, cross-dispersed slit) to check for any dependence on color. The whole experiment was then repeated twice more, overexposing by a factors 15 and 50, to study the residual effect of larger saturation factors. Nominal Gain 1 was used throughout.</p> <p>It turns out that the effect of saturation is negligible for the great majority of STIS CCD observations. Only the largest saturation factor (50X) had any observable effect on the dark current. The dark is found to be locally enhanced by (50 +/- 20)% over the nominal dark current in the first 300 sec. dark exposure after such a heavy (~50 X) saturation. The second dark image did not show any enhanced dark current (within the errors). There is no significant color effect. This is depicted in Figure 11, which shows a "G230LB spectrum" of the dark current, extracted from the first 300 s dark image taken right after the heaviest saturated G230LB spectrum at the location of the star. There was also no significant difference between the dark current measured after a heavy saturation in the UV vs. one in the red.</p> <p>Bias frames taken after heavily saturated images are not affected at all.</p>
Accuracy Archived	20% (on an effect of 50%, see above).
Continuation Plans	None.

Figure 11: Residual “G230LB spectrum” of the dark current taken right after a heavily saturated (50 times the A-to-D saturation level) G230LB spectrum of HD 149438. The “spectrum” of the dark current was extracted at the location of the star on the G230LB spectrum, and a median filter with a kernel of 5 pixels was applied to eliminate hot pixels and cosmic rays to some extent (some are still remaining, however). The nominal dark current level was subtracted before plotting. Note that there is no significant effect of the color of the light saturating the CCD on the (very small) residual dark current.



Proposal ID 8891: Test of STIS End of Slit Pseudo-Aperture Locations

Execution	This program's single visit executed on 29 Nov 2000.
Summary of Goals	Decreasing charge transfer efficiency in the STIS CCD has a detrimental effect on faint spectra acquired at the default location at the center of the chip. For signal levels of 50-100 e-, 10-15% of the charge can be lost during readout. For spectra of point sources and compact objects such as galactic nuclei, the full length of the slit is not needed. A target location closer to the read-out amplifier near the end of the slit can decrease the charge lost during parallel transfers by a factor of ~5. This proposal tested the implementation of new pseudo-apertures defined at row 900 on the CCD from the proposal-processing ground-system segment through the data calibration pipeline.
Summary of Analysis	<p>All target acquisitions and peakups were successful. The slews from the initial peakup were less than 0.1", while the slews on subsequent peakups at both the regular and E1 positions were less than 1 pixel. This indicates that the target was placed successfully in the E1 aperture, but suggests that the aperture positions could be improved.</p> <p>The spectra and images taken through the slit were compared with the expected positions. Table 7 summarizes the results for these spectra. The final column gives the ratio of counts observed at the E1 positions with each corresponding normal aperture position.</p> <p>The spectra and images taken through the E1 slit are all located near row 920 (row 900 + 20 for the overscan) in the raw image as expected. Variations of a few pixels are expected due to MSM non-repeatability. There is no obvious explanation for the relatively low count rates seen in the G750M spectra taken at the 52X0.05E1 and 52X0.1E1 positions.</p>
Accuracy Archived	See Table 7.
Continuation Plans	Cycle 10 programs 8929 "First-order LSFs for Pseudo-Aperture Locations" and 8928 "STIS PSFs at Pseudo-Apertures" will provide further calibration data for the E1 pseudo-aperture positions.

Table 7. The following table summarizes the results for these spectra. The final column gives the ratio of counts observed at the E1 positions with each corresponding normal aperture position.

Dataset	Aperture	Centroid	Counts	Percent
o6b601010	52X0.05 image	535.77,537.02	26265	
o6b601020	52X0.05 G750M	row 534		
o6b601030	52X0.05E1 image	538.67,921.35	17056	63%
o6b601040	52X0.05E1 G750M	row 916		
o6b601050	52X0.1E1 image	538.32,921.59	42148	85%
o6b601060	52X0.1E1 G750M	row 916		

Instrument Science Report STIS 2003-02

Dataset	Aperture	Centroid	Counts	Percent
o6b601070	52X0.1 image	535.77,537.02	49114	
o6b601080	52X0.1 G750M	row 533		
o6b601090	52X2 G430L	row 531		
o6b6010a0	52X2 image	536.57,537.02	61896	
o6b6010b0	52X2 G430L	row 529		
o6b6010c0	52X2E1 image	540.26,920.80	60171	97%
o6b6010d0	52X2E1 G430L	row 912		
o6b6010e0	52X0.5 G430M	row 555		
o6b6010f0	52X0.5 image	535.86,537.02	61217	
o6b6010g0	52X0.5E1 G430M	row 937		
o6b6010h0	52X0.5E1 image	539.24,920.03	59167	97%
o6b6010i0	52X0.2 G430M	row 553		
o6b6010j0	52X0.2 image	536.00,537.02	59476	
o6b6010k0	52X0.2E1 G430M	row 937		
o6b6010l0	52X0.2E1 image	539.38,920.21	54863	92%

Proposal ID 8843: MAMA Dark Monitor

Execution	Two exposures per week for each MAMA detector.
Summary of Goals	Monitor Dark Current of FUV and NUV MAMA detectors and look for changes in the characteristics of the dark current with time and temperature.
Summary of Analysis	<p>Statistics for both the NUV and FUV MAMA dark currents were routinely tabulated and posted under the STIS monitors web page.</p> <p><u>NUV MAMA:</u> The mean and standard deviation of the NUV dark count rate during this period was $1.35e-3 \pm 0.19e-3$ cnts/lo-res-pixel/sec. This totals to 1410 ± 203 cnts/sec over the entire detector. The mean OM2CAT temperature was 36.42 ± 1.55 C.</p> <p>New NUV MAMA darks have been constructed for several epochs. These new darks improve the flatness of dark subtracted images. An improved algorithm for temperature scaling of the darks at different times is under development and should be implemented during the next few months.</p> <p><u>FUV MAMA:</u> The FUV MAMA has been previously shown to exhibit an enhanced background glow in the upper left corner at high temperatures. This glow intensity correlates too poorly with time and temperature to allow pipeline subtraction. However, the glow is now more often present than not. The mean and standard deviation of the dark count rate in the glow region during this program were $5.8e-5 \pm 4.4e-5$ cnts/lo-res-pixel/second, while in the dark lower left corner, the rate was $6.6e-6 \pm 1.5e-6$ cnts/lo-res-pixel/sec. The mean OM1CAT temperature for these observations was 36.45 ± 1.49 C.</p> <p>An ISR describing the trends in the FUV and NUV MAMA darks is in preparation.</p>
Accuracy Archived	When periods following extended cooling of the NUV MAMA are excluded, the mean observed total NUV dark current varied between roughly 1100 and 1800 counts/sec.
Continuation Plans	Continued in Cycle 10 program 8920.

Figure 12: The measured NUV MAMA dark current as a function of temperature (open symbols) is compared to that predicted by the simple model implemented in the pipeline (solid line). The size of the symbols increases with the observation date.

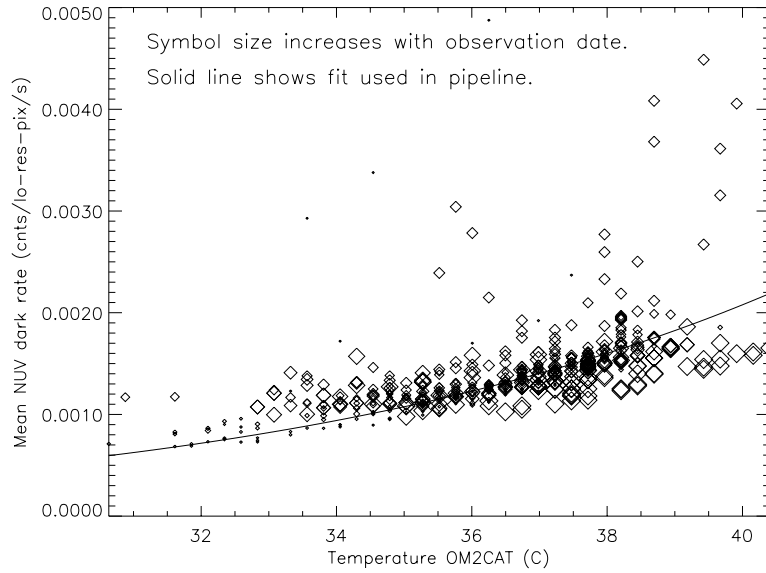
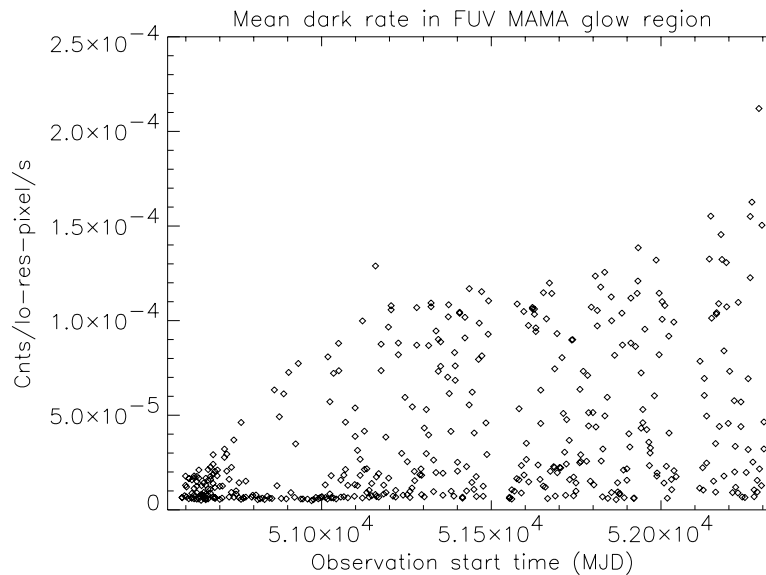


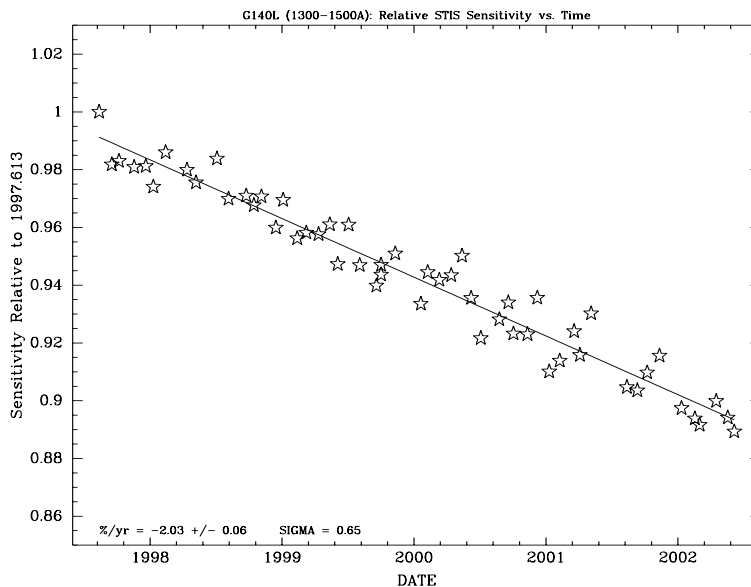
Figure 13: The mean dark current measured in the upper left (subarray [200:400,600:800] in a lo-res image) of the FUV MAMA detector is plotted as a function of time.

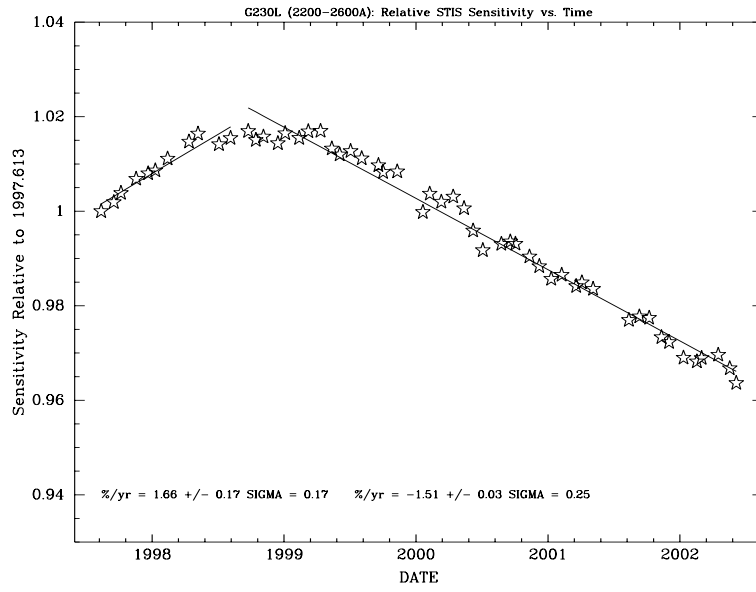


Proposal ID 8857: MAMA Sensitivity and Focus Monitor

Execution	Executed from September 2000 to August 2001. Planned 1 orbit monthly for L modes, 1 orbit every 2 months for M modes, and 2 orbits every 6 months for the echelles, for a total of 22 orbits. Two L and one M visits were lost and withdrawn due to the side-1 failure.
Summary of Goals	Monitor the sensitivity of each MAMA grating mode to detect any change due to contamination or other causes.
Summary of Analysis	Cumulative analysis of new data is maintained by David Stys. Previous trends continue. The rates of sensitivity loss for the FUV MAMA range from ~2%/yr (G140L) to ~2.5%/yr (G140M) and the NUV MAMA rates range from ~1%/yr (G230M) to ~1.5%/yr (G230L). Quantitative fits have been made to the trends in the L modes as functions of wavelength and epoch for incorporating them into the data reduction pipeline for both L and M modes. The SYNPHOT software has been updated to reflect these trends. Analysis of the echelle sensitivity is underway. A new ISR has been written and will be published upon review. Figure 14 summarizes the sensitivity trends for G140L and G230L. The slope, (i.e., percent-per-year change in sensitivity) and 1 sigma uncertainty in the linear fits are printed at the bottom of each plot as well as the rms(%) of the data residuals (SIGMA).
Accuracy Archived	The rms scatter is consistent with previous cycles, while the accuracy of the trend fits is higher due to the increasing temporal baseline (see ISR STIS 2001-01R).
Continuation Plans	Continued in Cycle 10 program 8919.

Figure 14: These two plots summarize the rates of sensitivity loss in the G140L and G230L modes due to contamination.





Proposal ID 8858: MAMA Full-Field Sensitivity

Execution	Two visits successfully completed in September 2000 and March 2001.
Summary of Goals	The purpose of this program is to monitor the sensitivity of the FUV- and NUV-MAMA detectors over the full field by observing the globular cluster NGC 6681. Photometry of many stars over the full field at epochs separated by approximately 6 months allows measurement of spatial and temporal variations in the sensitivity.
Summary of Analysis	Aperture photometry was performed on a subset of bright stars distributed over the field, as well as for specific horizontal branch stars for which spectra were obtained as part of Program 8422. To check the effect of sky background on the estimated magnitudes, different independent techniques were used to measure the sky.
Accuracy Archived	<p>FUV-MAMA (Clear) has a variation of 0.05 mag over the full field for magnitudes in the 15.9-18.8 range. This increases to ~0.10 mag at fainter magnitudes. See Figure 15 for a plot of this variation as a function of position on the FUV detector. As can be seen, this variation does not seem to be correlated with the position of a star on the detector.</p> <p>FUV-MAMA (Quartz) has a similar variation of ~0.04 from epoch to epoch, but shows a correlation between field orientation and the sign of the variation, that is, the magnitude for a given star is measured to be higher when the detector is oriented one way on the field, and lower when it is oriented the other way on the field. The FUV/Quartz is the only detector/filter combination where we see this correlation.</p> <p>NUV-MAMA (SrF2) has a variation of ~0.03 mag over the full field for magnitudes in the 16.2-17.0 range. See Figure 16 for a plot of this variation as a function of position on the NUV detector.</p>
Continuation Plans	Continued with some changes in Cycle 10 program 8918.

Figure 15: Each panel shows the difference between the mean magnitude and each measurement for a given star, plotted as a function of position of that measurement on the FUV-MAMA/25MAMA. The larger the circle, the larger the difference from the mean magnitude (with bins being <0.03 , 0.07 , 0.1 , 0.15 , 0.2 , >0.3).

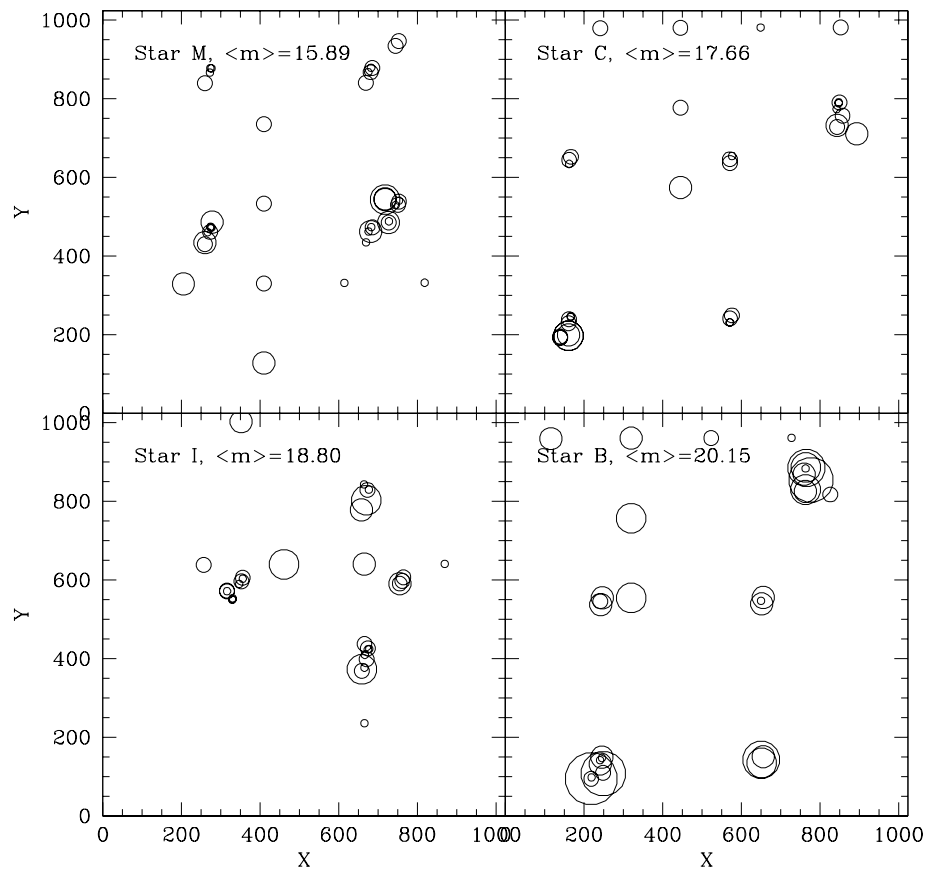
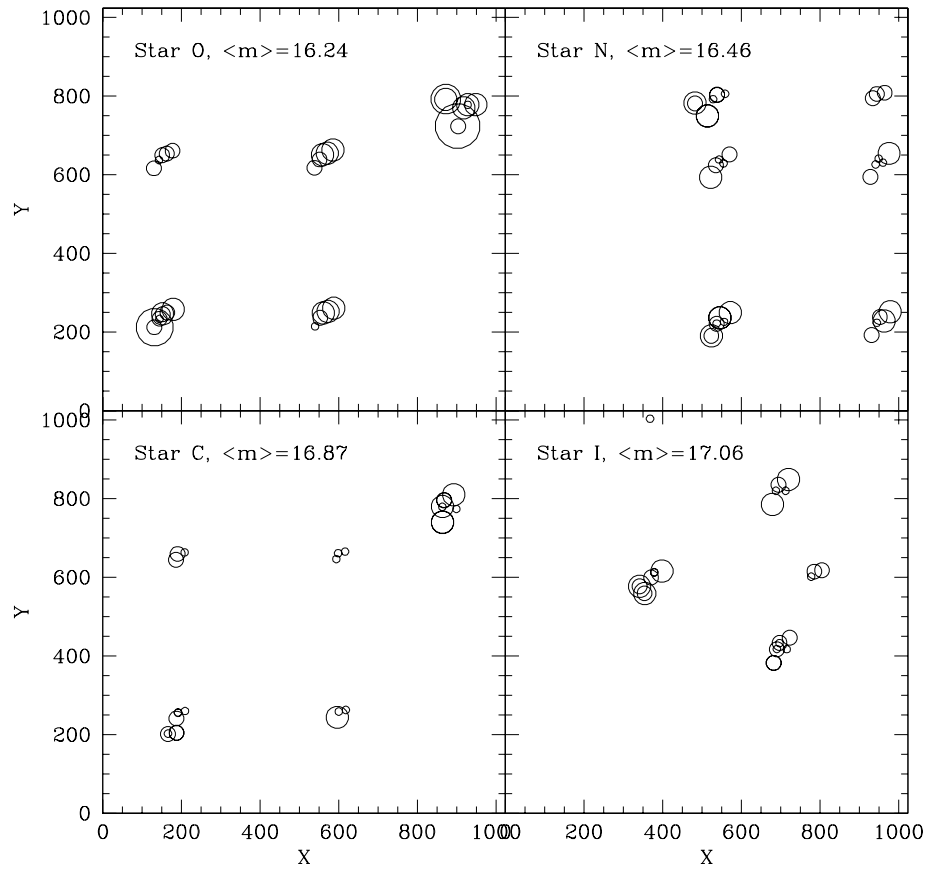


Figure 16: Each panel shows the difference between the mean magnitude and each measurement for a given star, plotted as a function of position of that measurement on the NUV-MAMA/F25SRF2. The larger the circle, the larger the difference from the mean magnitude (with bins being <0.01 , 0.03 , 0.07 , 0.1 , 0.15 , >0.2).



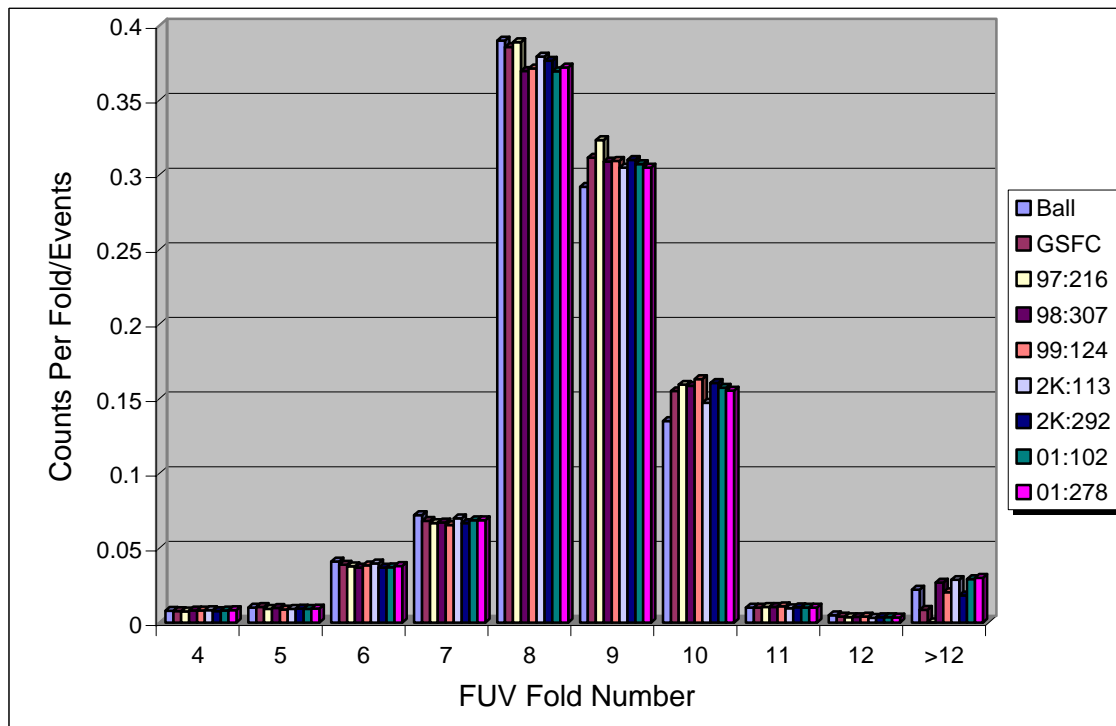
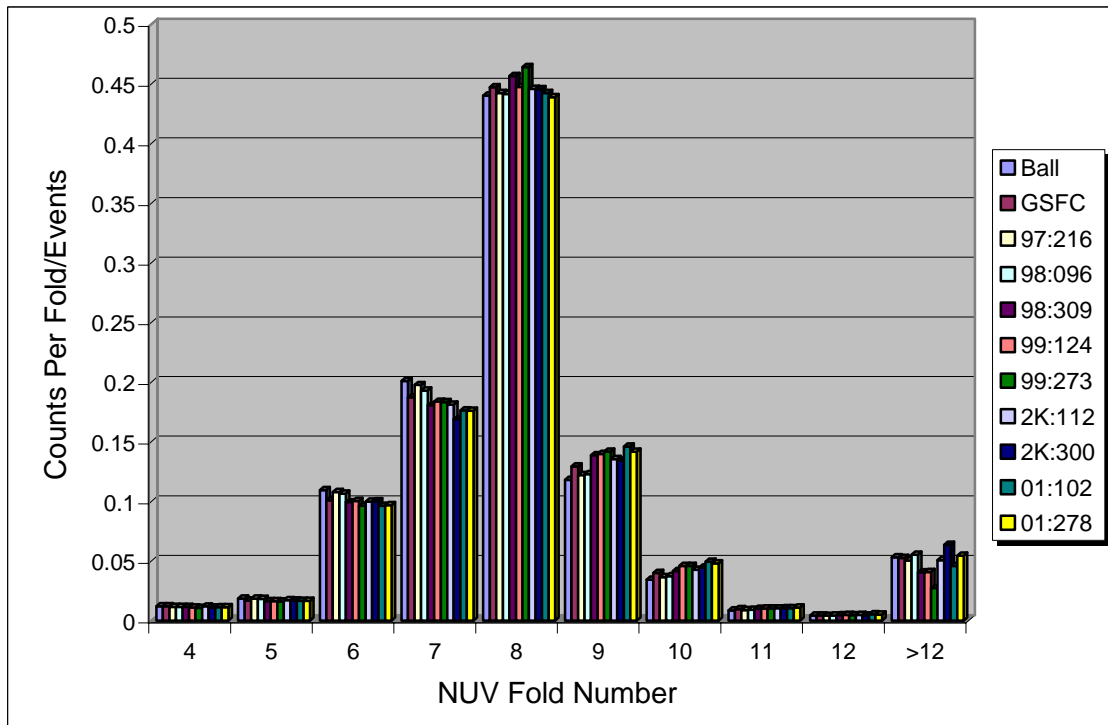
Proposal ID 8859: MAMA Dispersion Solutions

Execution	Program executed in July 2000. Note that the equivalent program (8917) in Cycle 10 executed in August 2001. These two programs span the full range of monthly offsets, because offsets are largest (but with opposite sign) for July and August.
Summary of Goals	For selected combinations of grating and central wavelength, determine empirical wavelength solutions from deep LINE lamp exposures. Compare with wavelengths predicted by Calstis, based on global shifts in the spectrum relative to the nominal location. Assess wavelength precision within a given exposure and accuracy relative to laboratory wavelengths.
Summary of Analysis	<p>Only echelle observations have been analyzed in detail. Observations were obtained with E140H (1271, 1416, 1598), E140M (1425), E230H (1813, 2263, 2762), and E230M (1978, 2707). For these deep exposures, accurate wavelength solutions were obtained with the IDL program ech_2dfit, using an FTS line list from NIST. The same datasets were also processed with Calstis versions 2.10 and 2.13, using "old" and "new" dispersion reference (DISPTAB) files. In the FUV and NUV, the old files were l2j01380o and l3m14381o, while the new files were m7p16110o and m7p16111o. The new DISPTAB files include updated dispersion coefficients for modes observed in this program, as well as new columns (YREF, MREF, and A4CORR) discussed below.</p> <p>The four separate reductions with Calstis were compared with the more accurate solution from ech_2dfit, expressing wavelength errors in terms of pixels. In all cases, errors vary systematically from one echelle order to the next. Calstis 2.12 and subsequent versions contain logic (by Don Lindler) to use new DISPTAB columns to correct approximately wavelength errors that vary systematically with order. Measured shifts in the cross-dispersion direction (SHIFTA2) are converted into order dependent wavelength shifts. The correction generally reduces errors, but is not perfect.</p> <p>With Calstis 2.10 and the old DISPTAB files, the maximum error is 1.8 pixels with a "typical" error (median of the absolute value of errors for all pixels) of 0.6 pixels. With Calstis 2.13 and the new DISPTAB files, the maximum error is 1.0 pixels with a typical error of 0.2 pixels. Thus, changes to Calstis and the new DISPTAB files together generally reduce echelle wavelength errors by a factor of 2 to 3. The maximum error is twice the value stated in the Instrument Handbook, but the typical error is half the accuracy listed in the Handbook.</p>
Accuracy Archived	Standard processing with the latest Calstis and DISPTAB files yields echelle wavelengths that are typically good to 0.2 pixels, but errors as large as 1 pixel are still possible, especially for the reddest and bluest orders in any given setting.
Continuation Plans	Cycle 10 program 8917 calibration data was obtained at the opposite extreme in MSM monthly offset. Cycle 11 should obtain calibration data with no offset and at all central wavelengths. It is likely that wavelength calibration could be improved by constructing DISPTAB files with a sequence of USEAFTER dates, but no resources should be allocated to this activity until ECF completes their effort to improve echelle wavelength solutions.

Proposal ID 8860: MAMA Fold Distribution

Execution	Visits executed on April 12 and October 5, 2001.
Summary of Goals	Measure the distribution of the charge cloud sizes incident upon the anode to monitor the health of the micro-channel plates.
Summary of Analysis	No degradation is apparent (see Figure 17). The STIS MAMA tubes remain in good health for those parameters measured by the fold analysis. The analysis is described by Long (2001). Procedures and requirements available in the TIR 97-09 and ISR 98-02 .
Accuracy Archived	Degradation is measured as a large (more than 20%) deviation between the current and previous measurements.
Continuation Plans	Continued in Cycle 10 program 8921.

Figure 17: The fold analysis measures the health of the MAMA micro-channel plate. When a photon strikes the MAMA detector it frees a single electron, which accelerates through the micro-channel plate and causes an avalanche of other electrons. The resultant cloud of electrons is collected at the coding electrodes and is interpreted as an event. The contribution of this electron cloud on the electrodes is referred to as the fold. Changes in the fold distribution would indicate a change in the condition of the MAMA tube. The plots for the NUV-MAMA (top) and FUV-MAMA (bottom) consistently show less than 3% change for the fold number distribution, confirming that the MAMA performance as monitored by the fold analysis has not degraded. The Ball Aerospace (Ball) and GSFC measurements are pre-launch (Long 2001).



Proposal ID 8862: MAMA FUV Flats

Execution	All planned exposures were successfully obtained in 10 visits between March and September of 2001. Visit 10 was significantly delayed by the loss of STIS side-1 electronics.
Summary of Goals	Determine the pixel-to-pixel response (p-flat) of the FUV detector, applicable to all FUV modes. Compare with the response derived in previous cycles, to look for time dependence. Co-add with data from previous cycles to improve S/N in the reference file, if warranted. Note that this program was intended to execute at one epoch, but there was a significant delay between visits due to the failure of side-1.
Summary of Analysis	New procedures and software were written to significantly improve the analysis of the p-flat data. This software was used to analyze all of the p-flat data from Cycles 7, 8, 9 and 10, creating a super p-flat. There was possible evidence for a small amount of time-variation, but co-adding the p-flats from each cycle gives the advantage of beating down the systematic errors introduced from the settings used in any single cycle. The analysis is summarized in STIS TIR 2002-03 .
Accuracy Archived	The counting statistics in the super p-flat give 0.5% accuracy, but the actual rms in extracted spectra is not significantly improved over that achieved using a p-flat from a single cycle, demonstrating the limitations of creating a p-flat from G140M data but using the p-flat for other spectroscopic modes (with different central wavelengths, dispersions, and detector incidence angles).
Continuation Plans	More data were obtained in Cycle 10 as part of program 8922, a continuation of program 8862. These data were included in the analysis above. More data will be taken in Cycle 11 as part of program 9624, after which the p-flat data should be taken with less frequency (given the practical limitations of the p-flat as the statistical significance is improved).

Proposal ID 8863: MAMA NUV Flats

Execution	All planned exposures were successfully obtained in 10 visits between March and August of 2001. Visits 8-10 were significantly delayed by the loss of STIS side-1 electronics.
Summary of Goals	Determine the pixel-to-pixel response (p-flat) of the NUV detector, applicable to all NUV modes. Compare with the response derived in previous cycles, to look for time dependence. Co-add with data from previous cycles to improve S/N in the reference file, if warranted. Note that this program was intended to execute at one epoch, but there was a significant delay between visits due to the failure of side-1.
Summary of Analysis	New procedures and software were written to significantly improve the analysis of the p-flat data. This software was used to analyze all of the p-flat data from Cycles 7, 8, 9 and 10, creating a super p-flat. There was possible evidence for a small amount of time-variation, but co-adding the p-flats from each cycle gives the advantage of beating down the systematic errors introduced from the settings used in any single cycle. The analysis is summarized in STIS TIR 2002-03 .
Accuracy Archived	The counting statistics in the super p-flat give 0.5% accuracy, but the actual rms in extracted spectra is not significantly improved over that achieved using a p-flat from a single cycle, demonstrating the limitations of creating a p-flat from G230M data but using the p-flat for other spectroscopic modes (with different central wavelengths, dispersions, and detector incidence angles).
Continuation Plans	More data were obtained in Cycle 10 as part of program 8923, a continuation of program 8863. These data were included in the analysis above. More data will be taken in Cycle 11 as part of program 9625, after which the p-flat data should be taken with less frequency (given the practical limitations of the p-flat as the statistical significance is improved).

Proposal ID 8849: Faint Standards Extension (FASTEX)

Execution	The eight visits of the predecessor proposal, CAL/STIS 8423, had executed successfully between February 2000 and November 2000. Eight of the ten visits of 8849 executed between September 2000 and August 2001. There was a guide star loss-of-lock during observations of WD0947+857 (visit 2), which resulted in this visit executing under single guide star tracking. This does not appear to have adversely affected the data quality, and no repeat was requested. Two other visits totaling to four orbits on NGC 6681 were delayed until June 2002 because of the 2001 STIS side-1 failure.
Summary of Goals	This program was implemented to extend the set of STIS flux standards to fainter magnitudes. Observations of the four FASTEX WDs will establish pure hydrogen spectrophotometric standards that are up to a factor of 1000 fainter than the primary WD standards and will support absolute flux calibrations for ACS, COS, and the astronomical community in general.
Summary of Analysis	All 36 spectra from the 24 orbits used in 8423 and 8849 to observe the four faint white dwarfs that are the primary targets of this program, have been reduced. One important result is the discovery that CTE losses in the G430L spectra cause up to a 7% discontinuity between the G230L and G430L spectra. CTE corrections have been investigated and one algorithm corrects the G230L-G430L flux discontinuity to better than 2%. More work is required to verify the general applicability of the preliminary CTE correction algorithm, to derive updated relative sensitivities for the +3/-3 arcsec positions for G140L, to update the time and temperature corrections, to verify the fundamental STIS sensitivities for the current set of observation of the four prime standards, and to analyze the spectra from the NGC 6681 observations.
Accuracy Archived	N/A
Continuation Plans	There was no follow on proposal during Cycle 10. Cycle 11 program 9631 adds even fainter standards for FASTEX.

References

- Arribas, S., Koekemoer, A., & Whitmore, B. 2003, *The 2002 HST Calibration Workshop; Hubble After the Installation of ACS and the NICMOS Cooling System*, (Baltimore: STScI), in press.
- Kimble, R. A., Goudfrooij, P. & Gilliland, R. L. 2000, SPIE, 4013, 532.

Appendix A

STIS Technical Instrument Reports (TIRs) and Instrument Science Reports (ISRs) produced from Cycle 9 data are listed below. A complete list of STIS ISRs is available from the STIS website at <http://www.stsci.edu/hst/stis/documents> (TIRs are intended for internal STScI use only, and cannot be accessed by outside users).

- STIS ISR 2001-01R** “Sensitivity Monitor Report for the STIS First-Order Modes-III (Revision A)”, D. J. Stys.
- STIS ISR 2001-03** “Temperature Dependence of the STIS CCD Dark Rate During Side-2 Operations”, T. M. Brown.
- STIS ISR 2003-01** “Absolute Flux Calibration of STIS MAMA Imaging Modes”, C. R. Proffitt.
- TIR 2002-03** “Revised Procedures for Creating MAMA P-Flats”, T. M. Brown.

STIS Cycle 9 calibration data also contributed to a number of presentations made at the 2002 HST Calibration Workshop, as well as to the following papers published in the proceedings of this workshop (Arribas, Koekemoer, & Whitmore, 2003).

- “STIS Calibration Status”, C. R. Proffitt & the STIS team.
- “Correcting STIS CCD Photometry for CTE Loss”, P. Goudfrooij & R. A. Kimble.
- “STIS Flux Calibration”, R. C. Bohlin.
- “STIS Echelle Blaze Shift Correction”, C. W. Bowers & D. Lindler.
- “Coronagraphic Imaging with HST and STIS”, C. A. Grady et al.
- “The STIS CCD Spectroscopic Line Spread Functions”, T. R. Gull et al.
- “STIS Status after the Switch to Side-2”, T. M. Brown & J. E. Davies.
- “Absolute Flux Calibration of STIS Imaging Modes”, C. R. Proffitt, J. E. Davies, T. M. Brown, & B. Mobasher.
- “Sensitivity Monitor Report for the STIS First-Order Modes”, D. J. Stys et al.